

Towards a Systematic Improvement of the Fixed-Node Approximation in Diffusion Monte Carlo for Solids

Anouar Benali,^{1, a)} Kevin Gasperich,² Kenneth D. Jordan,² Thomas Applencourt,³ Ye Luo,¹ M. Chandler Bennett,⁴ Jaron T. Krogel,⁵ Luke Shulenburger,⁶ Paul R. C. Kent,^{7, 8} Pierre-François Loos,⁹ Anthony Scemama,⁹ and Michel Caffarel^{9, b)}

¹⁾*Computational Sciences Division, Argonne National Laboratory, Argonne, IL 60439, United States*

²⁾*Department of Chemistry, University of Pittsburgh, Pittsburgh, Pennsylvania 15260, United States*

³⁾*Argonne Leadership Computing Facility, Argonne National Laboratory, Argonne, IL 60439, United States*

⁴⁾*Materials Science and Technology Division, Oak Ridge National Laboratory, Oak Ridge, TN 37831, United States^{c)}*

⁵⁾*Materials Science and Technology Division, Oak Ridge National Laboratory, Oak Ridge, TN 37831, United States*

⁶⁾*HEDP Theory Department, Sandia National Laboratories, Albuquerque, New Mexico 87185, USA*

⁷⁾*Center for Nanophase Materials Sciences, Oak Ridge National Laboratory, Oak Ridge, TN 37831, United States*

⁸⁾*Computational Sciences and Engineering Division, Oak Ridge National Laboratory, Oak Ridge, TN 37831, United States*

⁹⁾*Laboratoire de Chimie et Physique Quantiques, Université de Toulouse, CNRS, UPS, France*

^{c)} This manuscript has been authored by UT-Battelle, LLC under Contract No. DE-AC05-00OR22725 with the U.S. Department of Energy. The United States Government retains and the publisher, by accepting the article for publication, acknowledges that the United States Government retains a non-exclusive, paid-up, irrevocable, worldwide license to publish or reproduce the published form of this manuscript, or allow others to do so, for United States Government purposes. The Department of Energy will provide public access to these results of federally sponsored research in accordance with the DOE Public Access Plan (<http://energy.gov/downloads/doe-public-access-plan>).

While Diffusion Monte Carlo (DMC) has the potential to be an exact stochastic method for *ab initio* electronic structure calculations, in practice the fixed-node approximation and trial wavefunctions with approximate nodes (or zeros) must be used. This approximation introduces a variational error in the energy that potentially can be tested and systematically improved. Here, we present a computational method that produces trial wavefunctions with systematically improvable nodes for DMC calculations of periodic solids. These trial wavefunctions are efficiently generated with the configuration interaction using a perturbative selection made iteratively (CIPSI) method, which iteratively selects the most relevant Slater determinants from the full configuration interaction (FCI) space. By introducing a simple protocol combining both exact and approximate finite-supercell results and a controlled extrapolation procedure to reach the thermodynamic limit, we show accurate DMC energies can be obtained using a manageable number of Slater determinants. This approach is illustrated by computing the cohesive energy of carbon diamond in the thermodynamic limit using Slater-Jastrow trial wavefunctions including up to one million Slater determinants.

^{a)}Electronic mail: benali@anl.gov

^{b)}Electronic mail: caffarel@irsamc.ups-tlse.fr

I. INTRODUCTION

A faithful and quantitative first principles (*i.e.*, *ab initio*) description of the electronic structure of solids is one of the greatest challenges of material science. For weakly correlated materials (most simple metals, semiconductors, and insulators), modern approximations to exact density-functional theory (DFT),¹⁻³ and approximate many-body perturbation theory (MBPT) approaches (such as the *GW* approximation^{4,5} and the Bethe-Salpeter equation⁶⁻⁸) generally yield ground- and excited-state properties in good agreement with experiment.^{9,10} In sharp contrast, for strongly correlated systems (*e.g.*, transition metal oxides) for which electrons can no longer be treated as weakly interacting quasiparticles, the approaches mentioned above may dramatically fail, even qualitatively.^{11,12} Furthermore, even for weakly correlated systems, we lack practical approaches where the approximations can be quantified and the error systematically reduced. Designing efficient and general computational approaches with controlled and testable approximations is therefore of great interest.

Quantum Monte Carlo (QMC) methods have been developed to treat weakly through strongly correlated systems while invoking few approximations. These include variational Monte Carlo (VMC) and diffusion Monte Carlo (DMC) in continuous space^{13,14}, and full configuration interaction QMC (FCIQMC)^{15,16} and auxiliary field QMC (AFQMC)^{17,18} in determinant space. These methods utilize stochastic integration to help treat the complexity of the many-body electronic structure problem, and are applicable to both solids and isolated molecules. Importantly it is becoming possible to compare these and other many-body methods with each other on equivalent problems and to both validate their results and focus improvements.^{19,20} In this study we will focus on DMC, which is the most widely used QMC approach for calculating the electronic structure of solids.^{13,21} DMC enjoys a relatively low computational scaling with system size and is well adapted to massive parallelism.²²⁻²⁶ For bosons, DMC can deliver the exact energy to an arbitrarily small error. However, for fermionic problems, a naive DMC implementation is not stable in time.^{27,28} To address the fermion sign problem and correctly obtain the required fermionic symmetry, practical DMC calculations must rely on the fixed-node approximation: the fermionic constraints are fulfilled by imposing the zeros (nodes) of the wavefunction to be those of an approximate antisymmetric (fermionic) trial function. However, because these nodes are approximate, the DMC energy has a residual variational error, referred to as the fixed-node error. Devising an efficient strategy to improve the trial wavefunction nodes *in a systematic way* and, thus, coming closer to achieving a

genuine general from-first-principles theory, is one of the major challenges of DMC.

One advantage of real space QMC methods is their ability to flexibly use different forms of trial wavefunction. Since only the values and derivatives of the wavefunction are required there is no need in principle to choose forms that are suited for conventional numerical integration. While it is now standard to utilize sophisticated multideterminant trial wavefunctions in molecules, most solid state applications of DMC use a single (Slater) determinant (SD) trial wavefunction. A Jastrow factor is used to incorporate dynamical correlations and improve the wavefunction overall, but it does not change the nodes. Although SD-DMC calculations have proven valuable in addressing a wide range of problems in chemistry and materials science, for example obtaining near chemical accuracy in van der Waals binding^{29,30}, this accuracy is far from general. A potentially general strategy to address this problem, which has been successfully applied to atoms and molecules, is to employ multideterminant (MD) trial functions.^{31–34} However this requires an efficient method to generate the multideterminant expansion.

In this work, we present a scheme to perform multideterminant DMC calculations in solids using configuration interaction (CI) based trial functions. We employ a selected CI (SCI) approach in which only the most important Slater determinants from the full CI (FCI) space are identified and selected. As we will show, this approach defers the exponential wall of conventional CI calculations sufficiently to allow practical application to solids. In the case of atomic and molecular systems, several successful applications of SCI trial functions in DMC calculations have been reported.^{31,34–41} Here, we use the configuration interaction using a perturbative selection made iteratively (CIPSI) algorithm,⁴² as implemented in the `QUANTUM PACKAGE` code⁴³ to generate the trial functions for DMC calculations on periodic systems. This approach is illustrated by computing the cohesive energy of carbon diamond in the thermodynamic limit. We use the `QMCPACK` quantum Monte Carlo package^{25,26} for the DMC calculations. Although diamond is not a particularly challenging system with respect to the role of electron correlation, it is a valuable test system since its cohesive energy is accurately known and pseudopotential accuracy is not a major concern.

The paper is organized as follows. In Sec. II, the theoretical aspects of the approach are presented. A brief summary of the CIPSI method is given and its extension to the case of periodic systems is described in depth. The computational details are provided in Sec. III. Results for diamond, both at the single- and multideterminant levels, are reported and discussed in Sec. IV. Finally, some concluding remarks are given in Sec. V, including areas where further improvements are desired. Unless otherwise stated, atomic units are used throughout this paper.

II. THEORY

A. The CIPSI algorithm

In the present manuscript, the CIPSI algorithm developed for finite-size atomic or molecular systems is generalized to the case of periodic solids. CIPSI is one of the variants of the broad class of methods known as SCI. Selecting determinants in the CI space is a natural idea, and many SCI variants have been developed under various acronyms and implementations over the last five decades.^{31,34,36–38,42,44–77} SCI methods are ordinary CI approaches except that determinants are not chosen based on predetermined occupation or excitation criteria, but are instead selected step by step based on their estimated contribution to the FCI energy and/or wavefunction. It is a particularly successful approach since it is well-recognized that, in a predefined subspace of determinants [for example, single and double excitations with respect to the Hartree-Fock (HF) reference], only a small fraction of them make a non-negligible contribution to the wavefunction.^{56,78} Therefore, an *on-the-fly* selection of determinants has been proposed as soon as the late 1960's by Bender and Davidson,⁴⁴ as well as by Whitten and Hackmeyer.⁴⁵ The main advantage of SCI methods is that no *a priori* assumption is made on the type of determinants needed to describe the electronic correlation effects. Therefore, at the potentially greater price of a blind and automated calculation, an SCI calculation is less biased by the user's understanding of the problem's complexity (for example, when choosing the active space orbitals for a particular problem).

The CIPSI approach was developed in 1973 by Huron, Rancurel, and Malrieu.⁴² In recent years, two of us have revived this approach³¹ and developed a very efficient and massively parallel version of the algorithm which has been implemented in QUANTUM PACKAGE.⁴³ Briefly, at each iteration n , CIPSI selects some external determinants $|D_\alpha\rangle$ not present in the current zeroth-order wavefunction

$$|\Psi_0^{(n)}\rangle = \sum_I c_I^{(n)} |D_I\rangle, \quad (1)$$

where $|D_I\rangle$ is an internal determinant. Starting, for example, with the HF determinant at $n = 0$, the external determinants are selected using a criterion based on the estimated gain in correlation energy evaluated using second-order perturbation theory that would result from the inclusion of $|D_\alpha\rangle$. Denoting the second-order correction as

$$e_\alpha^{(n)} = \frac{|\langle \Psi_0^{(n)} | \hat{H} | D_\alpha \rangle|^2}{E_{\text{var}}^{(n)} - \langle D_\alpha | \hat{H} | D_\alpha \rangle}, \quad (2)$$

where

$$E_{\text{var}}^{(n)} = \frac{\langle \Psi_0^{(n)} | \hat{H} | \Psi_0^{(n)} \rangle}{\langle \Psi_0^{(n)} | \Psi_0^{(n)} \rangle} \quad (3)$$

is the variational energy of the wavefunction at the n th iteration, a number of external determinants associated with the greatest $e_\alpha^{(n)}$ are incorporated into the variational space and the Hamiltonian is diagonalized to give $|\Psi_0^{(n+1)}\rangle$ and $E_{\text{var}}^{(n+1)}$. In practice, the size of the variational wavefunction is roughly doubled at each iteration. Next, the second-order Epstein-Nesbet energy correction to the variational energy (denoted as $E_{\text{PT2}}^{(n)}$) is computed by summing up the contributions of all external determinants

$$E_{\text{PT2}}^{(n)} = \sum_{\alpha} e_{\alpha}^{(n)}, \quad (4)$$

and the total CIPSI energy is given by

$$E_{\text{CIPSI}}^{(n)} = E_{\text{var}}^{(n)} + E_{\text{PT2}}^{(n)}. \quad (5)$$

The algorithm is then iterated until some convergence criterion (for example, $|E_{\text{PT2}}^{(n)}| \leq \epsilon$) is met. For simplicity, in the following the superscript denoting the largest iteration number attained will be dropped from the various expressions. When the number of determinants in the variational space gets large, computing the second-order correction E_{PT2} by adding up all contributions e_α to the sum becomes computationally unfeasible. To perform this formidable task, a simple and efficient hybrid stochastic-deterministic algorithm has been developed.⁵⁹ In short, the leading contributions to the sum in Eq. (4) are exactly computed (deterministic part) while the very large number of small residual contributions are sampled via a Monte Carlo algorithm (stochastic part).

B. CIPSI for periodic systems

We now present the extension of CIPSI to periodic solids. As in any CI calculation, we must define (i) the system (number of electrons, charge and positions of the nuclei), (ii) the Hamiltonian, and (iii) the one-electron basis set. The calculation of the one- and two-electron integrals required for the computation of the Hamiltonian matrix elements then needs to be discussed.

1. Supercells

In practice, an infinite solid is modeled by a finite supercell obtained by replicating a given primitive cell n_i times in each Cartesian direction (*i.e.*, $i = x, y, z$). Accordingly, we will label a

supercell as $n_x \times n_y \times n_z$. In the present study, we will restrict ourselves to the simplest case of a cubic primitive cell of side L with arbitrary n_x , n_y , and n_z values. The supercell is then a rectangular cuboid of volume $\Omega = N \times L^3$, where $N = n_x n_y n_z$ is the total number of primitive cells replicated to build the supercell.

The supercell being defined, we are led back to an ordinary CI calculation consisting of the set of electrons and nuclei present in the supercell and subject to an external periodic electric potential. We denote \mathbf{R}_I and Z_I the position and charge of the I th nuclei of the primitive cell ($I = 1, \dots, N_n$). The actual system is then composed of $N \times N_n$ nuclei at positions $\mathbf{R}_I + t_a \mathbf{a} + t_b \mathbf{b} + t_c \mathbf{c}$, and of $N \times N_e$ electrons, where N_e is the number of electrons of the primitive cell. Here, $\mathbf{t} = t_a \mathbf{a} + t_b \mathbf{b} + t_c \mathbf{c} = (t_a, t_b, t_c)$ is the lattice translation vector, and the triplet of integers (t_a, t_b, t_c) takes all the values needed to generate the supercell through translations of the primitive cell along its unit vectors $(\mathbf{a}, \mathbf{b}, \mathbf{c})$. Similarly, the supercell translation vector is defined as $\mathbf{T} = T_A \mathbf{A} + T_B \mathbf{B} + T_C \mathbf{C} = (T_A, T_B, T_C)$, where, in the case of a cubic primitive cell, $(\mathbf{A}, \mathbf{B}, \mathbf{C}) = (L\mathbf{a}, L\mathbf{b}, L\mathbf{c})$ are the corresponding unit translation vectors of the supercell.

We emphasize that, in contrast to effective one-body theories such as HF or DFT, many-body electronic structure calculations explicitly taking into account the electron-electron interaction, such as the ones performed here, cannot be restricted to the primitive cell if accurate properties are to be obtained.¹³ In one-body theories the thermodynamic limit can be reached by indefinitely improving the \mathbf{k} -point sampling of the first Brillouin zone of the primitive cell. In presence of electron-electron interaction the translation of *individual* electrons is no longer a symmetry of the Hamiltonian (\mathbf{k} is no longer a good quantum number) and the use of supercells is mandatory (see, e.g., Refs 13 and 79 for a discussion of this aspect).

2. *Hamiltonian*

The supercell electronic Hamiltonian

$$\hat{H}_N = \hat{T} + \hat{V}_{ne} + \hat{V}_{ee} + \hat{V}_{nn} \quad (6)$$

has a standard form, except that the electron-electron, electron-nucleus, and nucleus-nucleus Coulombic potentials, \hat{V}_{ee} , \hat{V}_{ne} , and \hat{V}_{nn} , respectively, are now periodized to model the interaction of the electrons and nuclei belonging to the supercell with the infinite set of replicas associated with

their periodic images, *i.e.*,

$$\begin{aligned} \hat{H}_N = & -\frac{1}{2} \sum_i \nabla_i^2 - \sum_{\mathbf{T}} \sum_i \sum_J \frac{Z_J}{|\mathbf{r}_i - \mathbf{R}_J + \mathbf{T}|} \\ & + \frac{1}{2} \sum_{\mathbf{T}} \sum'_{ij} \frac{1}{|\mathbf{r}_i - \mathbf{r}_j + \mathbf{T}|} + \frac{1}{2} \sum_{\mathbf{T}} \sum'_{IJ} \frac{Z_I Z_J}{|\mathbf{R}_I - \mathbf{R}_J + \mathbf{T}|}, \end{aligned} \quad (7)$$

where \mathbf{r}_i is the position of the i th electron, $\sum_{\mathbf{T}} \equiv \sum_{T_A=-\infty}^{\infty} \sum_{T_B=-\infty}^{\infty} \sum_{T_C=-\infty}^{\infty}$, and the prime symbol indicates that the self-interaction term $i = j$ or $I = J$ has to be excluded when $\mathbf{T} = \mathbf{0} = (0, 0, 0)$.

As is well known, periodic Coulomb potentials are mathematically ill-defined due to the long-range character of the Coulomb interaction. The periodic infinite sums in Eq. (7) not only converge very slowly but they are also conditionally convergent, meaning that the result depends on the order of summation. A specific and careful mathematical treatment has to be introduced in order to provide a meaningful answer. The standard solution, and the one we employ here for the three Coulomb potentials in Eq. (7), is to resort to the Ewald summation technique.

Applying the Ewald summation technique, for example, to the nucleus-nucleus term \hat{V}_{nn} in Eq. (7) enables one to compute this term as a sum of two contributions: a short-range contribution in real space and a short-range in reciprocal space. Both contributions are expressed as rapidly converging infinite sums, thus leading to a very fast and efficient calculation of the potential. Explicitly, it is given by

$$\begin{aligned} \hat{V}_{\text{nn}} = & \frac{1}{2} \sum_{\mathbf{T}} \sum'_{IJ} \frac{Z_I Z_J}{|\mathbf{R}_I - \mathbf{R}_J + \mathbf{T}|} \operatorname{erfc} \left[\frac{|\mathbf{R}_I - \mathbf{R}_J + \mathbf{T}|}{\sqrt{2}\sigma} \right] \\ & + \frac{2\pi}{\Omega} \sum_{\mathbf{G} \neq \mathbf{0}} \frac{e^{-\frac{\sigma^2 k^2}{2}}}{k^2} \left| \sum_I Z_I e^{i\mathbf{G} \cdot \mathbf{R}_I} \right|^2 - \frac{\sum_I Z_I^2}{\sqrt{2\pi}\sigma} - \frac{\pi\sigma^2}{\Omega} \left(\sum_I Z_I \mathbf{R}_I \right)^2, \end{aligned} \quad (8)$$

where $\operatorname{erfc}(x)$ is the complementary error function, \mathbf{G} refers to the set of quantized reciprocal vectors of the supercell defined by the condition $e^{i\mathbf{G} \cdot \mathbf{T}} = 1$, and σ is a small positive parameter chosen to facilitate convergence. Additional details can be found, for example, in Refs. 80 and 81.

3. Basis functions

In this work, the one-electron basis functions are chosen to be crystalline Gaussian-based atomic orbitals

$$\chi_{\mu\mathbf{k}}(\mathbf{r}) = \sum_{\mathbf{T}} e^{i\mathbf{k} \cdot \mathbf{T}} \tilde{\chi}_{\mu}(\mathbf{r} + \mathbf{T}), \quad (9)$$

i.e., the periodized (or translationally-symmetry-adapted) version of the (localized) Gaussian atomic orbitals $\tilde{\chi}_\mu(\mathbf{r})$ from the supercell. In Eq. (9), the crystal momentum vector \mathbf{k} is chosen within the first Brillouin zone of the primitive cell, and it is sampled from a Monkhorst-Pack grid,⁸² an evenly-spaced rectangular grid in reciprocal space [see Sec. (II C)]. The atomic index μ is referred to as the band index after periodization.

The molecular orbitals of the system are then defined as

$$\phi_{p\mathbf{k}}(\mathbf{r}) = \sum_{\mu}^{N_{\text{bas}}} C_{\mu p}(\mathbf{k}) \chi_{\mu\mathbf{k}}(\mathbf{r}), \quad (10)$$

where N_{bas} is the number of basis functions, and the molecular orbital coefficients $C_{\mu p}(\mathbf{k})$ are now momentum-dependent due to the translational-symmetry adaptation of the basis functions. Once again, we emphasize that, because of the explicit treatment of the electron-electron interaction, \mathbf{k} is no longer a good quantum number and the orbitals defined above do not have the correct translational symmetry of the problem. However, choosing such a representation is particularly convenient in practice since it allows to take full advantage of the techniques and codes developed for the effective one-particle theories, such as HF and DFT.

4. One- and two-electron integrals

The Hamiltonian and the one-electron basis set having been defined, the next step in a CI calculation is to evaluate the Hamiltonian matrix elements between Slater determinants. This requires evaluation of one- and two-electron integrals. It is easy to see from the expressions of the Hamiltonian [see Eqs. (7) and (8)] and basis functions [see Eq. (9)] that this can be accomplished by calculation of the integrals over Fourier transforms of product of Gaussian functions for which fast and reliable algorithms have been developed.^{83–85}

The only new aspect with respect to standard CI implementations is the use of complex-valued orbitals, integrals and Hamiltonian matrix elements. Let us denote the two-electron integrals as

$$\langle p\mathbf{k}_p q\mathbf{k}_q | r\mathbf{k}_r s\mathbf{k}_s \rangle = \iint_{\Omega^2} d\mathbf{r}_1 d\mathbf{r}_2 \phi_{p\mathbf{k}_p}^*(\mathbf{r}_1) \phi_{q\mathbf{k}_q}^*(\mathbf{r}_2) \frac{1}{r_{12}} \phi_{r\mathbf{k}_r}(\mathbf{r}_1) \phi_{s\mathbf{k}_s}(\mathbf{r}_2). \quad (11)$$

Since the one-particle basis functions are invariant with respect to the primitive lattice translation vectors \mathbf{t} , the two-electron integrals must conserve crystal momentum, *i.e.*, $\mathbf{k}_p + \mathbf{k}_q = \mathbf{k}_r + \mathbf{k}_s + \mathbf{g}$, where \mathbf{g} is a reciprocal lattice vector of the primitive cell.

When real-valued orbitals are used, a given two-electron integral is symmetric with respect to permutations of the orbital indices p and r , or q and s , as well as with the permutation of the electron labels 1 and 2, thus resulting in a 8-fold symmetry of the set of two-electron integrals. Consequently, the N_{bas}^4 four-index integrals can be mapped to a set of approximately $N_{\text{bas}}^4/8$ unique integral values.⁸⁶ However, when one considers complex-valued orbitals, the integral $\langle p\mathbf{k}_p q\mathbf{k}_q | r\mathbf{k}_r s\mathbf{k}_s \rangle$ is no longer invariant with the permutations of p and r , or q and s , so the number of unique integral values scales as $N_{\text{bas}}^4/2$ (exchanging the electron indices 1 and 2 still leaves the value of the integral unchanged). When storing these complex-valued integrals, it is useful to recognize that exchanging p with r , or q with s changes the integral value in a non-trivial way. However, exchanging both of these pairs simultaneously yields the complex conjugate of the original value, *i.e.*, $\langle p\mathbf{k}_p q\mathbf{k}_q | r\mathbf{k}_r s\mathbf{k}_s \rangle^* = \langle r\mathbf{k}_r s\mathbf{k}_s | p\mathbf{k}_p q\mathbf{k}_q \rangle$. This allows one to save an additional factor of two in the storage requirements; one then only needs to store $N_{\text{bas}}^4/4$ complex-valued two-electron integrals.

5. *Hamiltonian matrix elements*

In order to implement FCI or any of its lower-cost alternatives, one must be able to evaluate matrix elements of the Hamiltonian in the space of Slater determinants. If the determinants are all built from the same set of orthonormal spin-orbitals (which is the case here), then one can evaluate matrix elements via the usual Slater-Condon rules (see, *e.g.*, Ref. 86 and Ref. 87 for an efficient implementation in a determinant-driven context).

C. **Boundary conditions and twist averaging**

In order to reduce finite-size effects and, to accelerate the convergence to the thermodynamic limit (*i.e.*, $N \rightarrow \infty$), it is advantageous to exploit the freedom in the type of periodic boundary conditions of the supercell. By judiciously choosing the electron momenta \mathbf{k} of the basis functions [see Eq. (9)], the boundary conditions can be easily implemented. Translating one electron of the supercell by a superlattice vector (say, $\mathbf{A} = L\mathbf{a}$) generates a phase factor, $e^{iL\mathbf{k}\cdot\mathbf{a}}$, for each of the orbitals of the CI determinants. Accordingly, a global phase factor common to all determinants is obtained whenever all these individual phase factors are made equal, that is

$$e^{iL\mathbf{k}_1\cdot\mathbf{a}} = e^{iL\mathbf{k}_2\cdot\mathbf{a}} = \dots = e^{i\theta}, \quad (12)$$

where θ is some arbitrary angle (or twist) between $-\pi$ and π . These conditions are fulfilled when momenta are chosen uniformly spaced in the first Brillouin zone of the lattice (that is, by using a Monkhorst-Pack grid⁸²) and shifted by a common vector \mathbf{K}

$$\mathbf{k}_{i_a} = \mathbf{K} + \frac{i_a}{t_a} \frac{\mathbf{b} \times \mathbf{c}}{\mathbf{a} \cdot (\mathbf{b} \times \mathbf{c})}, \quad (13a)$$

$$\mathbf{k}_{i_b} = \mathbf{K} + \frac{i_b}{t_b} \frac{\mathbf{c} \times \mathbf{a}}{\mathbf{b} \cdot (\mathbf{c} \times \mathbf{a})}, \quad (13b)$$

$$\mathbf{k}_{i_c} = \mathbf{K} + \frac{i_c}{t_c} \frac{\mathbf{a} \times \mathbf{b}}{\mathbf{c} \cdot (\mathbf{a} \times \mathbf{b})}, \quad (13c)$$

with $i_l = 0, \dots, t_l$ ($l = a, b, c$) is the twist index. In this case, we have $|D\rangle \rightarrow e^{i\theta} |D\rangle$, with $\theta = \mathbf{K} \cdot \mathbf{a}$. Boundary conditions can be varied with θ from $-\pi$ to $+\pi$, $\theta = 0$ and $\theta = \pm\pi$ corresponding to periodic and anti-periodic boundary conditions, respectively.

For a given system size, a property O can be computed by averaging out its values for different \mathbf{K} values (or twists θ). In the limit of an infinite set of sampling values, we have

$$\langle O \rangle = \frac{1}{2\pi} \int_{-\pi}^{\pi} d\theta \langle \Psi_\theta | \hat{O} | \Psi_\theta \rangle, \quad (14)$$

where Ψ_θ is the exact wavefunction of the system for the corresponding boundary condition. In practice, the integral is computed as a finite sum over shifted Monkhorst-Pack grids, as expressed by Eqs. (13a), (13b), and (13c). The main effect of twist-averaging is to suppress the major part of the one-body shell effects in the filling of single-particle states. Note that each value of θ requires an independent calculation, the total computational cost is then proportional to the number of twists.

III. COMPUTATIONAL DETAILS

The DMC method is employed to compute ground-state energies within the fixed-node approximation. The application of DMC to solids being now well documented, we refer the interested reader to the existing literature for the theoretical background (see, for example, Refs. 13, 25, and 79). Calculations were performed using QMCPACK.^{25,26} The integrals over periodized Gaussian-type orbitals are carried out using the PySCF program,⁸⁸ which has been interfaced with QUANTUM PACKAGE.⁴³

To model carbon diamond, we used a primitive cell with two carbon atoms separated by 1.545 Å (approximately, 3.568 Å for the lattice constant). In order to compute the cohesive energy in the thermodynamic limit and to correct energies for finite-size effects, we consider supercells made of

16 ($2 \times 2 \times 2$), 54 ($3 \times 3 \times 3$) and 128 ($4 \times 4 \times 4$) atoms with converged twist-averaged (TA) boundary conditions with a total of 216, 64 and 27 twists respectively.⁸⁹ All calculations are carried out using the Burkatzki-Filippi-Dolg (BFD)^{90,91} effective core potentials and the associated $2s2p1d$ or $3s3p2d1f$ contracted Gaussian-type orbital (GTO) basis sets (BFD-vDZ or BFD-vTZ, respectively). Both SD-DMC and MD-DMC calculations used a time step of 0.001 a.u. and Casula’s T-moves for pseudopotential localization.⁹²

The trial wavefunctions for DMC consist either of a single determinant or multideterminant expansion determined using CIPSI multiplied by a Jastrow factor with one, two, and three body terms. The parameters for the one- and two-body terms were represented by B-splines and the three-body term by a polynomial. These parameters were optimized in VMC through a variant of the linear method of Umrigar *et al.*⁹³ Note that the coefficients of the CIPSI expansion were not optimized in VMC and therefore in this study the nodal surface is wholly determined by the CIPSI expansion.

IV. RESULTS

A. Single-determinant fixed-node DMC

To establish a reference for the multideterminant studies we first investigate the dependence of single determinant DMC energies on the initial orbitals and their basis sets. In Fig. 1, we show the dependence of the fixed-node DMC energy for single determinant trial wavefunctions built with LDA⁹⁴, PBE⁹⁵, B3LYP^{96–99} and HF orbitals calculated with the BFD-vDZ and BFD-vTZ basis sets. These calculations were performed for the simplest case of a single primitive cell consisting of two carbon atoms ($1 \times 1 \times 1$ supercell), with the SD-DMC energy being computed at the Γ point. As an additional reference, the SD-DMC energy obtained using LDA orbitals expanded in a large plane-wave (PW) basis set with a high energy cutoff of 175 hartree and the same pseudopotential is also reported. Using a larger energy cutoff of 250 hartree leads to a difference in DMC energies below 1 millihartree and therefore our initial choice of 175 hartree is close to the complete basis set limit. Note that the fixed node SD-DMC energies using nodal surfaces of the Kohn-Sham determinants obtained from different DFT approximations differ by less than the variation in the pure DFT energies, 6.8(6) millihartree vs 13.05 millihartree, respectively. The SD-DMC energies obtained with LDA orbitals expanded in the BFD-vTZ and PW basis sets coincide within 1(6) millihartree

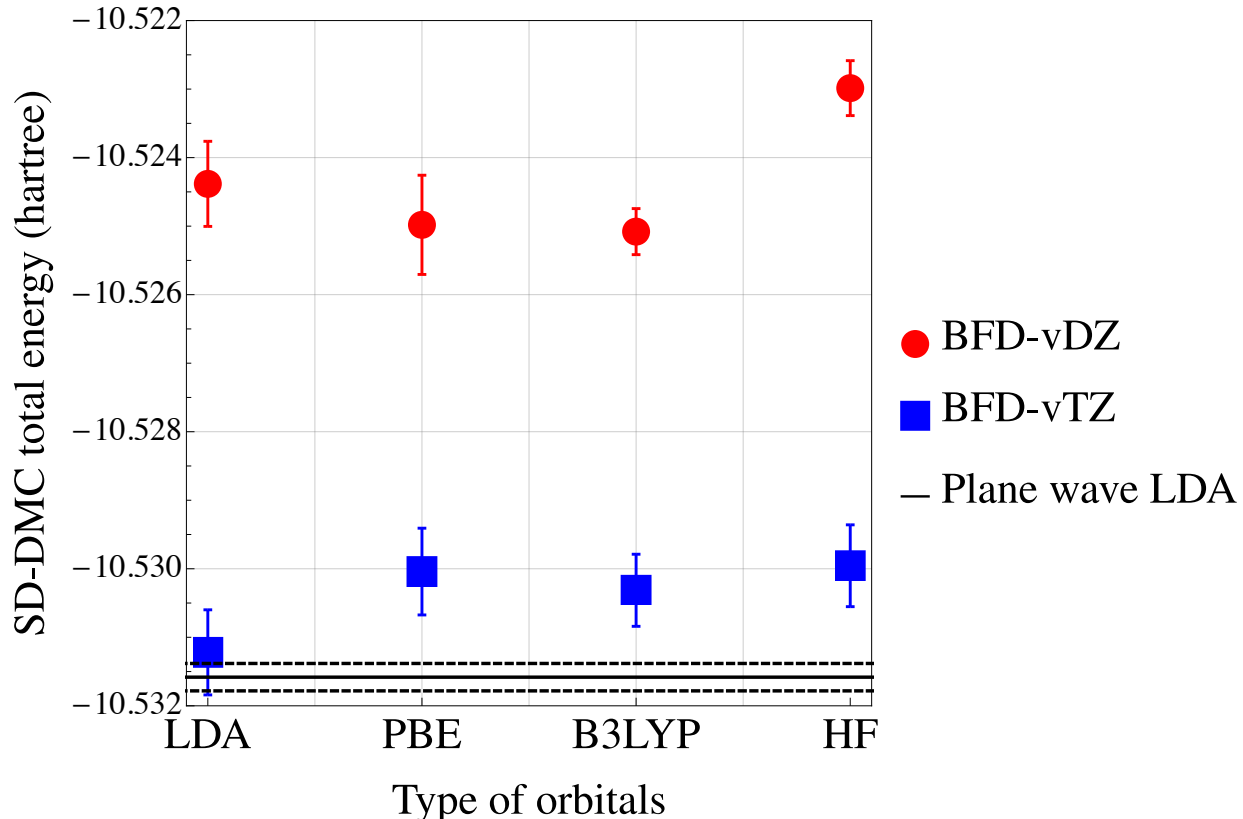


FIG. 1. SD-DMC total energy of the $1 \times 1 \times 1$ diamond primitive cell computed at the Γ point using SD trial wavefunctions built with various orbitals (LDA, PBE, B3LYP, and HF) and the BFD-vDZ (blue) or BDF-vTZ (red) GTO basis sets. The solid line corresponds to the SD-DMC energy obtained using a large PW basis set and LDA orbitals and the dashed lines indicate the associated statistical error. The raw data can be found in the [supplementary material](#).

thus indicating the suitability of the BFD-vTZ basis set. On the other hand, an appreciably higher SD-DMC energy is obtained when using the BFD-vDZ basis set. Consequently, in the following, all calculations are performed with the BFD-vTZ basis set.

In Table I, we report twist-averaged SD-DMC total energies (per primitive cell) as a function of the supercell size N , as well as the corresponding cohesive energies. We also report the SD-DMC energies computed by Shin *et al.* in Ref. 100, which were obtained using a PW basis set and a single Slater determinant wavefunction of PBE orbitals and using the same twist values.¹⁰¹ Results are compared to our SD-DMC data using B3LYP orbitals and the BFD-vTZ basis set. The SD-DMC total energies from the two calculations are very close, with a difference never greater than 3 millihartree. Electronic cohesive energies calculated by subtracting from the crystal energy the SD-

TABLE I. Twist-averaged SD-DMC total energies (in hartree/cell) and cohesive energies (in hartree) of diamond for supercells of increasing size $N = n^3$ ($n = 2, 3$, and 4). The (extrapolated) thermodynamic values and the cohesive energies (with and without ZPE correction) are also reported.

Cell size ($n \times n \times n$)	SD-DMC (B3LYP/GTO) ^a	SD-DMC (PBE/PW) ^b
$2 \times 2 \times 2$	-11.4217(1)	-11.4199(1)
$3 \times 3 \times 3$	-11.4078(7)	-11.4049(1)
$4 \times 4 \times 4$	-11.4020(5)	-11.3995(1)
Extrapolated ($N \rightarrow \infty$) ^c	-11.3971(7)	-11.3949(1)
Cohesive energy (w/o ZPE)	0.2772(4)	0.2755(1)
Cohesive energy (w/ ZPE)	0.2712(4)	0.2695(1)

^a Results from the present work obtained with B3LYP orbitals and the BFD-vTZ GTO basis set.

^b Results from Ref. 100 obtained with PBE orbitals and a PW basis set.

^c Extrapolated values obtained using a quadratic fit.

DMC energy of the isolated atoms calculated using the same approaches [$-5.4226(2)$ hartree/atom for PBE/PW and $-5.42138(2)$ hartree/atom for B3LYP/GTO] lead to a difference of only 3.0 ± 0.4 millihartree once extrapolated to the thermodynamic limit. Adding the zero-point vibrational energy (ZPE) correction estimated to be 6.0 millihartree/atom¹⁰² brings the SD-DMC(B3LYP/GTO) cohesive energy to 1.3 ± 0.4 millihartree of the estimated experimental value¹⁰³ of 0.2699 hartree (see Table I). The result indicates that there is very good error cancelation between the bulk and atomic total energies at the single determinant level in carbon diamond.

B. Multideterminant trial wavefunctions

In Fig. 2, we show the convergence of the CIPSI variational energy E_{var} and its second-order corrected value $E_{\text{var}} + E_{\text{PT2}}$ as a function of the number of determinants in the reference space (see Sec. II A) for the $1 \times 1 \times 1$ diamond primitive cell at the Γ point and using the BFD-vTZ basis set. Independent calculations using both HF and B3LYP orbitals are shown. Despite the large size of the Hilbert space (about $\sim 10^{11}$ determinants), energy convergence is achieved with a reasonable accuracy using less than $\sim 10^7$ determinants. In addition, the FCI limit is independent on the orbital

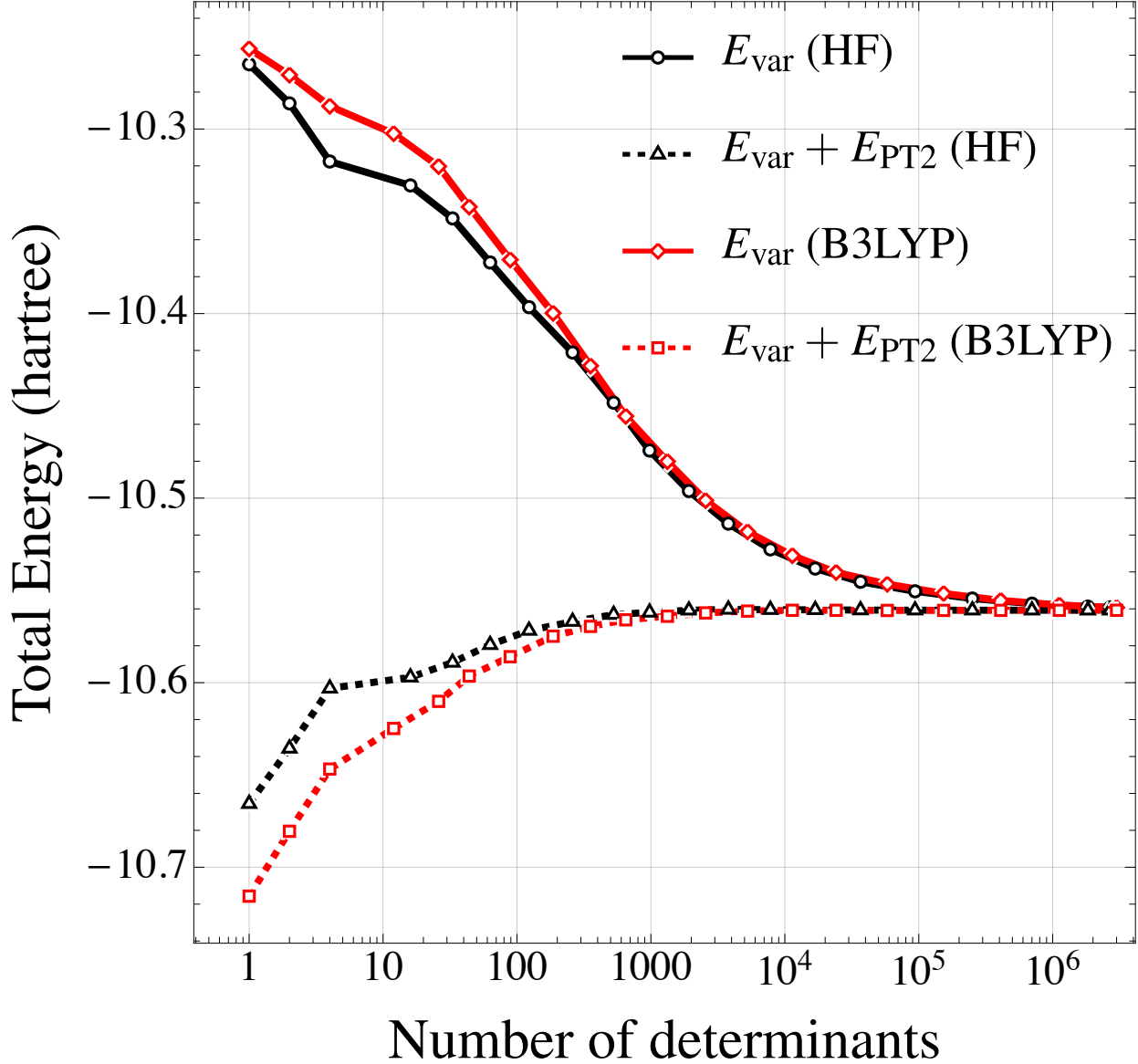


FIG. 2. Convergence of the CIPSI energies with the size of the variational space for the $1 \times 1 \times 1$ diamond primitive cell computed at the Γ point. Both the CIPSI variational energy E_{var} and its second-order corrected value $E_{\text{var}} + E_{\text{PT2}}$ (dashed) computed with the BFD-vTZ basis set using HF orbitals (black) and B3LYP orbitals (red) are reported. The raw data can be found in the [supplementary material](#).

set employed in the SCI calculation, as it should be. In the variational calculations, convergence to millihartree accuracy is achieved at about 3×10^6 determinants whether using HF or B3LYP orbitals. When the perturbative corrections to the energy are included, millihartree accuracy is reached with only $\sim 2 \times 10^3$ and $\sim 4 \times 10^3$ determinants for HF and B3LYP orbitals, respectively.

Although CIPSI rapidly converges to the FCI limit for the $1 \times 1 \times 1$ supercell (Γ point calcula-

tions) the exponential character of the FCI approach is still present and, for larger supercells, the number of determinants required to reach the FCI limit to the required accuracy rapidly becomes computationally intractable. To alleviate this issue and to enable treating larger supercells we limit the SCI calculations to a subset of orbitals belonging to a pre-defined active space (CAS-CI). Of course, there are many ways of choosing such an active space. Here, we consider the simplest approach where only virtual orbitals with one-electron energies below a given energy threshold are included in the active space. This is a reasonable choice since the high-energy orbitals are expected to have a small impact on the wavefunction and, thus, on the location of the nodes.

Figure 3 illustrates the use of such a CAS-CI. The error in DMC total energy (in hartree/atom) computed at the Γ point as a function of the number of orbitals belonging to the active space is presented. The error is calculated with respect to the converged DMC value obtained with 58 orbitals. For the $1 \times 1 \times 1$ primitive cell, results are reported for both B3LYP and HF orbitals, and for a number of orbitals in the CAS-CI up to the maximum of 58. For the $2 \times 1 \times 1$ supercell, only the B3LYP results are presented, and the maximum number of orbitals in the CAS-CI corresponds to only half of the total number of orbitals (116). For the $1 \times 1 \times 1$ supercell a well converged SD-DMC energy is achieved when using only 30 of the 58 B3LYP orbitals, but all orbitals must be retained to obtain a well converged result when using HF orbitals. For the larger $2 \times 1 \times 1$ cell for which the CAS-CI is built with B3LYP orbitals, convergence to within 1.0 ± 0.3 millihartree/atom is reached between 30 and 40 orbitals out of a total of 116. Due to the better convergence of the calculations with truncated orbital spaces when using B3LYP than HF orbitals, B3LYP orbitals are used in all subsequent calculations.

C. Multideterminant fixed-node DMC

Figure 4 illustrates one of the central points of this work, namely the possibility of improving nodal surfaces in a systematic way using SCI multideterminant trial wavefunctions. Fixed-node DMC total energies using various SD and MD trial wave functions are represented in Fig. 4 for the $1 \times 1 \times 1$ diamond primitive cell. On the left side of the graph, DMC energies obtained with SD trial wavefunctions built with LDA, PBE, B3LYP, and HF orbitals, respectively, are reported. (These are the same as the BFD-vTZ results reported in Fig. 1.) At the scale of the figure 4, the various SD-DMC energies are very similar, and are much higher in energy than the MD-DMC energies, which are up to 0.05 hartree lower. This indicates a significant improvement in the quality

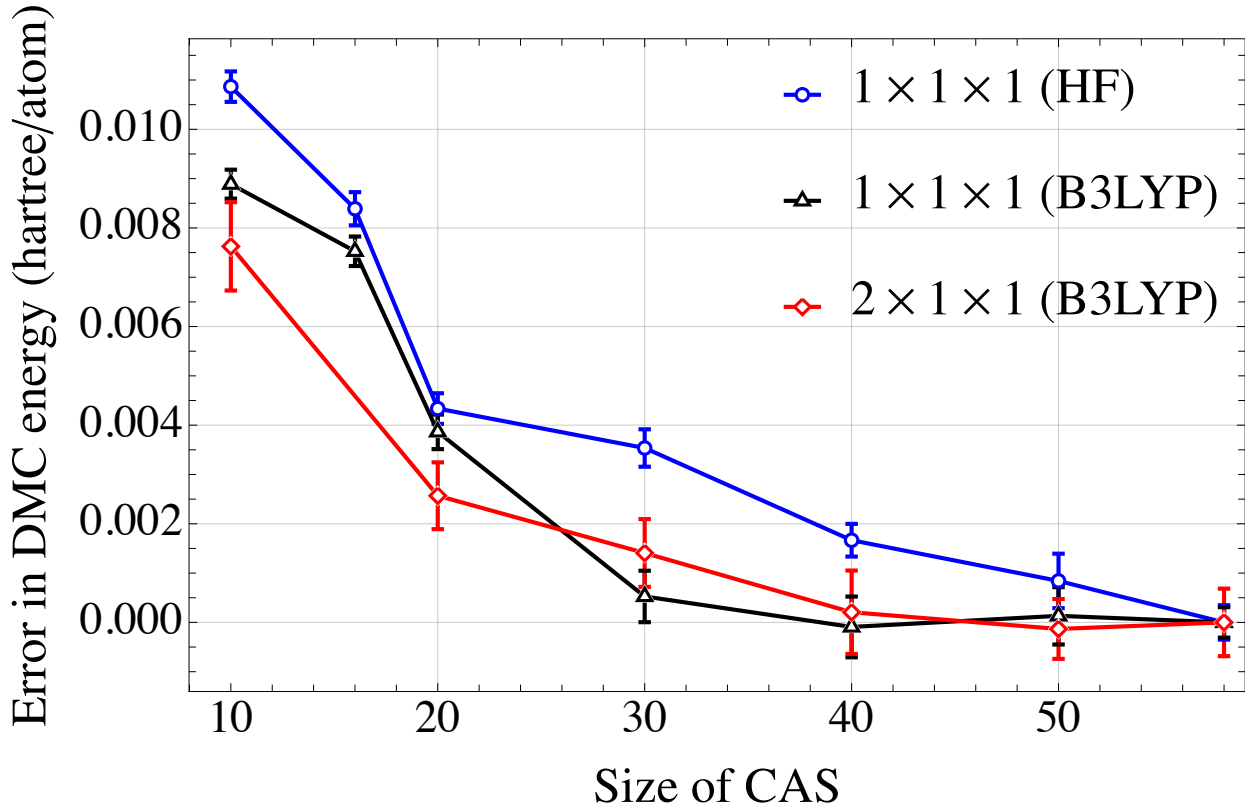


FIG. 3. Error in the DMC total energy (in hartree/atom) computed at the Γ point as a function of the number of orbitals in the active space for CAS-CI trial wavefunctions built with HF orbitals ($1 \times 1 \times 1$ cell) or B3LYP orbitals ($1 \times 1 \times 1$ and $2 \times 1 \times 1$ cells). These calculations are performed with the BFD-vTZ basis set. The raw data can be found in the [supplementary material](#).

of the nodal surface. On the right side of the graph, the convergence of the MD-DMC energy as a function of the size of the CIPSI expansion is presented both using the FCI (lower black curve) and CAS-CI (upper blue curve) spaces. The corresponding numerical data (including the number of determinants and the intrinsic variance) are reported in Table II. Here, ϵ is a threshold associated with the number of determinants retained in the expansion, and $\epsilon = 0$ corresponds to the full CIPSI wavefunction (which is much smaller than the FCI space due to a limit on the total number of determinants retained, see Ref. 104). In view of the computational cost of using a very large number of determinants in the trial wavefunction in DMC calculations, it is important to limit the determinants used to the smallest number possible. As seen in Table II the fixed-node energies are essentially converged within statistical errors at $\epsilon = 10^{-5}$ and, thus, to consider the full CIPSI wavefunction ($\epsilon = 0$) in DMC is not necessary here. Note that the number of determinants needed

TABLE II. DMC total energies (in hartree/cell) computed at the Γ point for the $1 \times 1 \times 1$ diamond primitive cell as a function of the truncation threshold ϵ on the coefficients of the CIPSI wavefunction computed within the full CI space and the restricted CAS-CI space with the BFD-vTZ basis set. For both spaces the final CIPSI wave function is obtained by stopping the selection process when the number of determinants exceeds about 1 million. The number of determinants in the trial wavefunction and intrinsic variance in the energy are also reported for each value of ϵ as well as the variance of the energy inferred from the DMC data.

Truncation threshold ϵ	FCI space			CAS-CI space		
	# determinants	DMC energy	Variance	# determinants	DMC energy	Variance
10^{-2}	178	-10.5638(3)	0.2428(4)	200	-10.5633(2)	0.2399(5)
10^{-3}	4124	-10.5707(3)	0.2010(1)	3204	-10.5694(3)	0.1950(2)
10^{-4}	80864	-10.5791(4)	0.1730(2)	57990	-10.5754(7)	0.1720(2)
10^{-5}	738998	-10.5812(3)	0.1382(7)	578025	-10.5776(4)	0.16384(5)
10^{-6}	1043197	-10.5817(4)	0.1372(8)	1282995	-10.5788(8)	0.16338(9)
$\epsilon = 0$	1137782	-10.5817(7)	0.1363(8)	1510556	-10.5796(9)	0.16260(2)

to reach a given threshold ϵ is smaller for the FCI space than the CAS-CI space. This results from the greater flexibility available with the FCI space. The convergence curves of the MD-DMC energy both for the FCI and CAS-CI spaces are similar and, at near-convergence, the two DMC energies differ by only about 2 ± 1 millihartree. The intrinsic variance in the energy shows a systematic improvement with the number of determinants in the expansion when using the FCI space.

As seen from Fig. 4 the DMC energy decreases monotonically and smoothly when increasing number of determinants in the trial wavefunction. As discussed in Ref. 38, there is no guarantee that increasing the number of Slater determinants in the trial wavefunction lowers the DMC energy, because the selection procedure does not explicitly optimize the nodal surface and DMC energy. However in all applications performed so far – atoms^{31,39,104}, molecules^{35–38,58}, and now solids – a systematic decrease of the fixed-node DMC energy is observed whenever the SCI trial wavefunction is improved variationally, upon increasing the number of determinants, the size of the basis set, or the size of the active space.

The DMC total energy (in hartree/cell) of diamond as a function of $1/N$, where N is the size of the system, *i.e.*, the total number of primitive cells replicated to create the supercell ($N = 8, 18, 27$, and 64 for $2 \times 2 \times 2, 3 \times 3 \times 2, 3 \times 3 \times 3$, and $4 \times 4 \times 4$, respectively), computed with

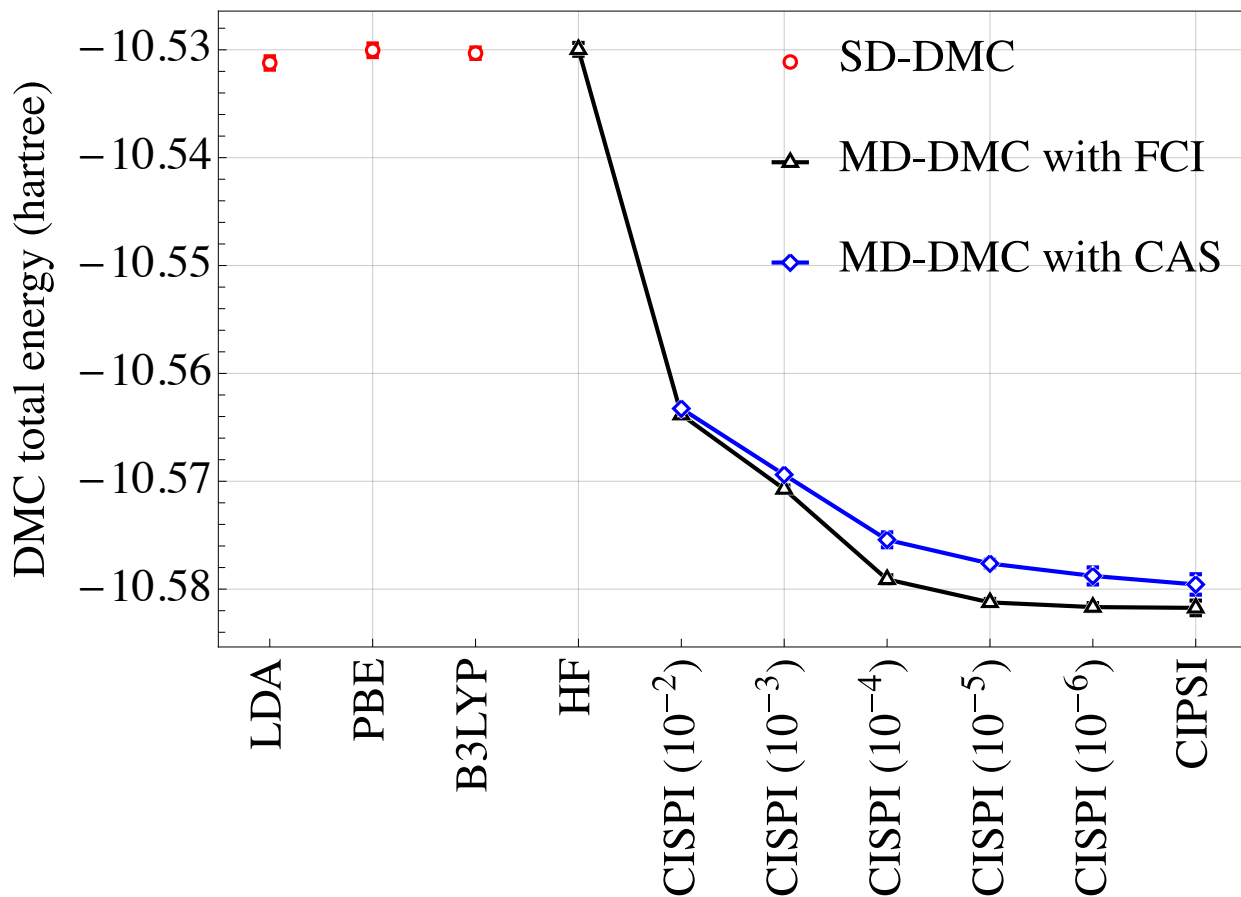


FIG. 4. Comparison of DMC total energies (in hartree) computed at the Γ point with various SD and MD trial wave functions for the $1 \times 1 \times 1$ diamond primitive cell. The SD-DMC energies (red dots) are computed with trial wave functions built with LDA, PBE, B3LYP, and HF orbitals. The MD-DMC energies are given as a function of the size of the CIPSI expansion for the FCI space which contains 58 orbitals (black curve) and the CAS-CI space which contains 30 orbitals (blue curve). The multideterminant trial wavefunctions are built with B3LYP orbitals obtained with the BFD-vTZ basis set. Numbers in parentheses on the abscissa correspond to the values of the truncation threshold ϵ (see text). Error bars are either smaller or of the order of the size of the markers. The raw data are gathered in Table II and in the [supplementary material](#).

various methods and approximations is reported in Fig. 5. The two upper curves (solid lines) report SD-DMC (red) and MD-DMC (black) energies computed at the Γ point. The two lower curves (dashed lines) are SD-DMC (red) and MD-DMC (black) energies obtained by twist-averaging as described in Sec. II C. To minimize the statistical fluctuations we re-optimized the Jastrow factor at each twist. The number of determinants in the multideterminant trial wavefunction varies from about 600000 to 1200000.

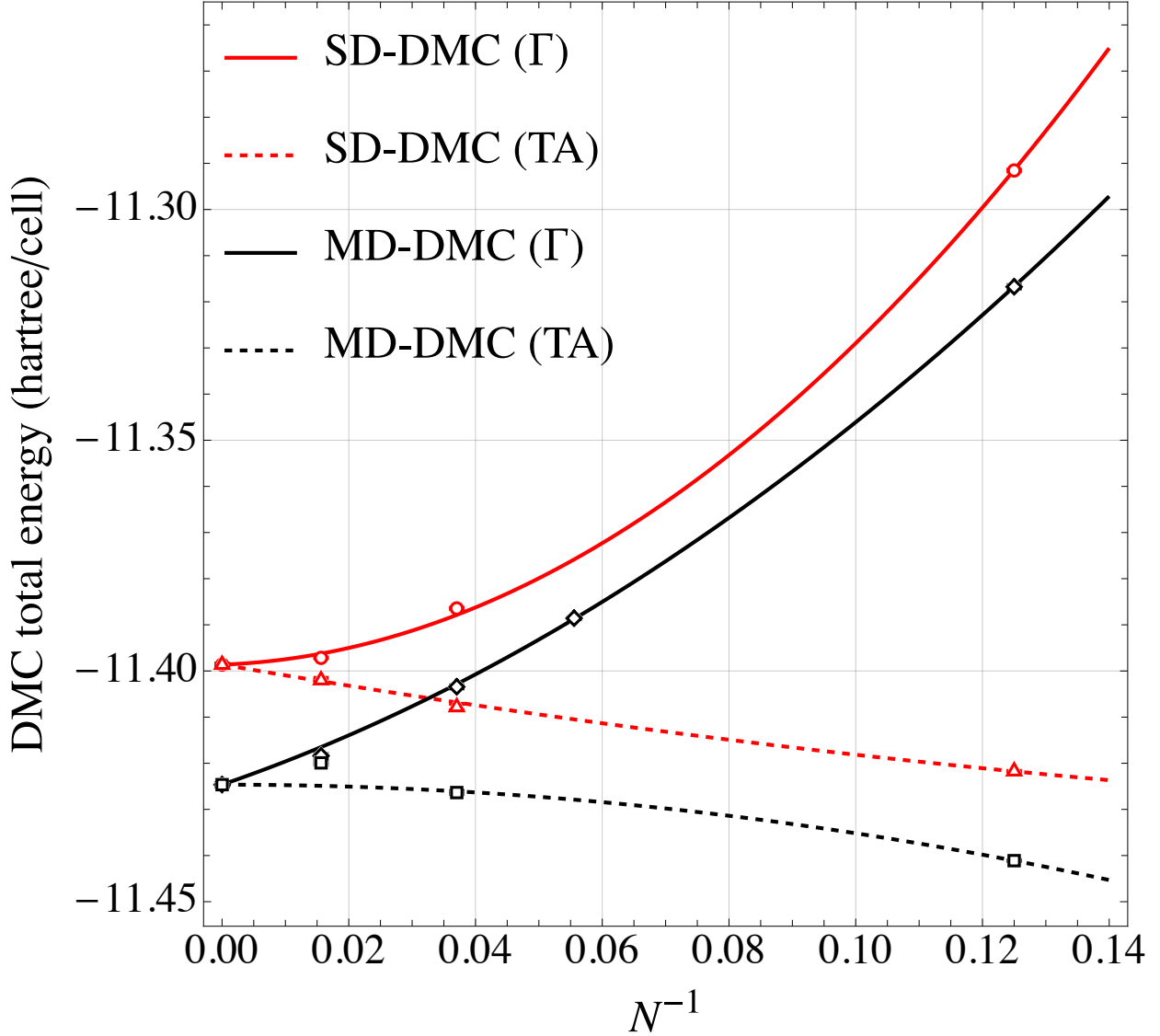


FIG. 5. SD- and MD-DMC total energies (in hartree/cell) as a function of the inverse of the system size N . Energies are calculated either at the Γ point (Γ , solid lines) or by twist-averaging (TA, dashed lines). Error bars are either smaller or of the order of the size of the markers. Each set of energies [SD (red lines) or MD (black lines)] are fitted simultaneously using Eq. (16a) or Eq. (16b). The raw data can be found in the [supplementary material](#).

SD-DMC calculations (at the Γ point and twist-averaged) have been performed for the $2 \times 2 \times 2$, $3 \times 3 \times 3$, and $4 \times 4 \times 4$ supercells. MD-DMC calculations are much more computationally demanding than their SD-DMC analogues. Consequently, MD-DMC calculations have been limited to the $2 \times 2 \times 2$ and $3 \times 3 \times 3$ supercells, with the energy of the $4 \times 4 \times 4$ supercell being estimated as

explained below. In all cases we only computed the symmetry inequivalent twists in the Brillouin zone, using symmetries to reduce the number of expensive DMC calculations. There are 16, 8, and 4 inequivalent twists out of 216, 64, and 27 total for the $2 \times 2 \times 2$, $3 \times 3 \times 3$, and $4 \times 4 \times 4$ supercells, respectively.

To further reduce the computational effort, an approximate version of the twist-averaged MD-DMC energies was employed for the $3 \times 3 \times 3$ and $4 \times 4 \times 4$ superlattices. In this procedure we estimate the energy at a given twist (other than Γ) via

$$E_{\text{DMC}}(w_i) \approx E_{\text{DMC}}(w_0) + E_{\text{HF}}^{\text{B3LYP}}(w_i) - E_{\text{HF}}^{\text{B3LYP}}(w_0), \quad (15)$$

where w_i denotes the i th twist (w_0 being the Γ point) and $E_{\text{HF}}^{\text{B3LYP}}$ is the energy computed with the HF energy functional and B3LYP orbitals. This approximation relies on the B3LYP band structure being sufficiently accurate, but can be further improved by considering how this data is extrapolated to the thermodynamic limit, as we will detail below.

Fig. 6 reports the SD- and MD-DMC energies computed both exactly and using Eq. (15) for the 16 independent twists of the $2 \times 2 \times 2$ supercell. To facilitate the visualization of the actual differences between data, the 16 DMC energies are artificially connected with straight lines. The two upper (red) curves and the two lower (black) curves correspond to SD-DMC and MD-DMC calculations, respectively. As one can see, there is excellent agreement between the exact (solid lines) and approximate (dashed lines) treatment of twist averaging in the case of SD-DMC. For MD-DMC, the agreement is not as good but remains satisfactory for the present purpose.

We can estimate the twist-averaged DMC energy of the $4 \times 4 \times 4$ supercells by combining the extrapolated value of the DMC energy at the Γ point and a twist-averaged contribution from Eq. (15). The extrapolated value reported in Fig. 5 has been obtained as the value resulting from a quadratic fit of the three values corresponding to the Γ point energies of the $2 \times 2 \times 2$, $3 \times 3 \times 3$, and $4 \times 4 \times 4$ supercells.

Finally, we can exploit the fact that both Γ point and twist-averaged energies must converge to the same value in the thermodynamic limit (*i.e.*, $N \rightarrow \infty$). This property is used as a constraint when fitting *simultaneously* both sets of energies with quadratic expressions, *i.e.*,

$$E_{\text{fit}}^{\Gamma}(N) = E_{\text{DMC}}^{N \rightarrow \infty} + \frac{c_1^{\Gamma}}{N} + \frac{c_2^{\Gamma}}{N^2}, \quad (16a)$$

$$E_{\text{fit}}^{\text{TA}}(N) = E_{\text{DMC}}^{N \rightarrow \infty} + \frac{c_1^{\text{TA}}}{N} + \frac{c_2^{\text{TA}}}{N^2}. \quad (16b)$$

The 5 parameters in Eqs. (16a) and (16b), *i.e.*, $E_{\text{DMC}}^{N \rightarrow \infty}$ and the four c_i 's, are obtained by minimizing the χ^2 -type function

$$\chi^2 = \sum_i \left[\frac{E_{\text{DMC}}^\Gamma(N_i) - E_{\text{fit}}^\Gamma(N_i)}{\delta E_{\text{DMC}}^\Gamma(N_i)} \right]^2 + \sum_i \left[\frac{E_{\text{DMC}}^{\text{TA}}(N_i) - E_{\text{fit}}^{\text{TA}}(N_i)}{\delta E_{\text{DMC}}^{\text{TA}}(N_i)} \right]^2, \quad (17)$$

where the δE_{DMC} 's are the corresponding statistical errors, and the sum runs over $N_i = 8, 18, 27$, and 64 for the Γ point energies (centered grid), and $N_i = 8, 27$, and 64 for the twist-averaged (TA) energies. The quantity $E_{\text{DMC}}^{N \rightarrow \infty}$ represents the best estimate of the DMC energy in the thermodynamic limit.

Following this extrapolation procedure, the SD-DMC total energy in the thermodynamic limit is found to be $E_{\text{SD-DMC}}^{N \rightarrow \infty} = -11.3986(2)$ hartree. Combined with the atomic SD-DMC total energy of $-5.4214(2)$ hartree, it yields a cohesive energy (including the ZPE contribution) of $0.2719(3)$ hartree, an estimate close to the value of $0.2712(4)$ hartree obtained by a simple quadratic fit of the DMC energies computed at the Γ point (see Table I). In the multideterminant case, we find $E_{\text{MD-DMC}}^{N \rightarrow \infty} = -11.4246(4)$ hartree, and using the atomic MD-DMC energy computed at $-5.4335(1)$ hartree obtain a ZPE-corrected cohesive energy of $0.2729(1)$ hartree. This value compares quite well with the estimated experimental cohesive energy of 0.2699 hartree extracted from Ref.¹⁰³. While this value is also similar to that obtained with single-determinant wavefunctions, there has been a significant lowering in the supercell and atomic energies due to use of multideterminant trial wave functions. In particular the energy of the atom obtained from the MD-DMC calculations is essentially exact (for the chosen pseudopotential).

It should be emphasized that comparing calculated and experimental cohesive energies is subject to the error made in estimating the ZPE contribution. The value of 6.0 millihartree/atom employed in this work was obtained by Schimka *et al.* using a zero-point anharmonic expansion based on DFT energy calculations¹⁰². For internal consistency and better accuracy, evaluating the ZPE correction using the very same DMC methodology would be desirable. A number of earlier *ab initio* calculations of the diamond cohesive energy have been reported in the literature. Values obtained using DMC with a single-determinant Slater-Jastrow trial wavefunction [$0.2699(2)$ hartree from Hood *et al.*¹⁰⁵ and $0.2702(4)$ hartree from Shin *et al.*¹⁰⁰] agree closely with the estimated experimental value of 0.2699 hartree. The CCSD calculations of McLain *et al.*⁸⁵ and Booth *et al.*¹⁶ give significantly smaller values of the cohesive energy, namely 0.2527 hartree and 0.2621 hartree, respectively. Finally, at the CCSD(T) level, 0.2712 hartree was reported by Booth *et al.*¹⁶. In our calculations, because the cohesive energy of the solid is slightly too large and the pseudoatom

is solved essentially exactly, the remaining difference with the experimental data must lie with a combination of the uncertainties in the extrapolation, timestep error in the DMC calculations, or pseudopotential construction and evaluation. The ZPE error is also sizable compared to the residual difference from experiment in all of the literature predictions.

For the $2 \times 2 \times 2$ supercell containing 16 carbon atoms, it is also instructive to compare our results to those of López Ríos *et al.*¹⁰⁶ using the nodes of an optimized backflow (BF) trial wavefunction. The pseudopotentials used are different, making a direct comparison of the energies not possible, although they are both around -11.4 hartree per primitive cell (see Table X of Ref.106 and data in our [supplementary material](#)). The BF wavefunction improves the DMC energy by approximately 0.007 hartree per primitive cell over the single-determinant result. A truncated expansion of 65 determinants in our Γ point CIPSI DMC yields a reduction of 0.011 hartree per primitive cell. A larger expansion of e.g. about 10^6 determinants, achieves a 0.0253(5) hartree improvement over the SD result per primitive cell.

V. CONCLUSIONS

We have demonstrated the feasibility of fixed-node DMC calculations for periodic solids using large multideterminant trial wavefunctions built from SCI expansions. Using as an example carbon diamond, this procedure is shown to be able to improve *systematically* the nodal surface of the trial wavefunction. In particular, we have found that the fixed-node DMC energy decreases monotonically and smoothly as a function of the number of determinants in the trial wavefunction. The cohesive energy of diamond obtained here is in close agreement with the experimental estimate.

Performing DMC calculations using large CI expansions together with large supercells is not feasible without further approximations due to overall cost. Here, this issue was addressed by introducing an approximate, yet well-defined, protocol combining both exact and approximate results for finite supercells and a controlled fitting procedure to reach the thermodynamic limit. Although approximate, our estimate of the diamond cohesive energy is, to the best of our knowledge, the first example of a fully *ab initio* MD-DMC calculation of a periodic solid. In our protocol, only the Jastrow parameters are optimized in the VMC step, with the linear coefficients of the CIPSI expansions being kept fixed. The main motivation for not optimizing the coefficients is to exploit the property of SCI methods to provide in a simple, well-defined (linear optimization), and systematic way of generating sequences of wavefunctions of increasing quality leading to

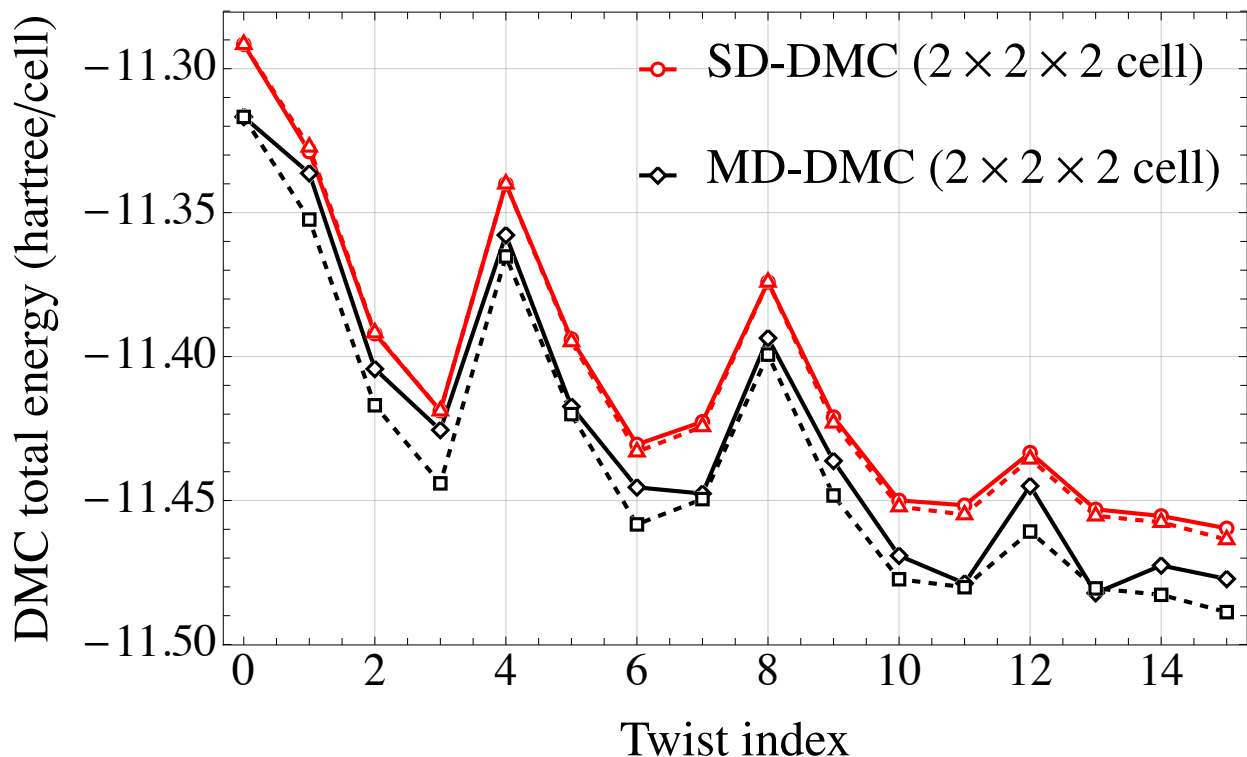


FIG. 6. Twist-averaged SD-DMC (red) and MD-DMC (black) total energies (in hartree/cell) for the $2 \times 2 \times 2$ supercell as a function of twist index (16 independent twists out of the 216 reciprocal grid). Solid and dashed lines correspond to exact and approximate calculations [using Eq. (15)], respectively. The DMC energies at the various twist indices are connected by straight lines only to guide the eyes. The raw data can be found in the [supplementary material](#).

a systematic reduction of the fixed-node error (see, Figs. 3 and 4). Defining such sequences is important, for example when extrapolating fixed-node energies at different supercell sizes or computing an energy difference such as the cohesive energy. However, the computational cost of using (very) large CI expansions in DMC calculations is high and strategies for generating more compact expansions are certainly desirable. Based on multideterminant DMC studies for isolated molecules (see, for example, Refs. 107,108, and 41) a practical solution consists of optimizing the CI coefficients in presence of the Jastrow factor and keeping only the most important determinants. However, such optimizations are challenging because the parameters in the Jastrow factors enter non-linearly and the objective function that one must minimize is evaluated stochastically. From a more general perspective, it would also be desirable to investigate the comparative performance with other types of trial wavefunctions including those with backflow as introduced by P. López

Ríos et al.¹⁰⁶ (a first numerical comparison is presented in this work) or of geminal forms.¹⁰⁹

Finally, we note that, to exploit the full potential of the present approach, more challenging materials must be investigated. In addition, it would be instructive to compute physical properties other than the cohesive energy that would potentially display a different dependence on the nodal error. We hope to be able to address these points in future studies.

SUPPLEMENTARY MATERIAL

See the [supplementary material](#) for the raw data associated with each figure of the manuscript.

VI. DATA AVAILABILITY STATEMENT

The data that supports the findings of this study are available within the article and its supplementary material.

ACKNOWLEDGMENTS

Authors are grateful to Drs. Peter Doak and Qiming Sun for debugging and code implementations enabling simulations in respectively QMCPACK and PySCF. AS, PFL, and MC were supported by the ANR PhemSpec project, grant ANR-18-CE30-0025-02 of the French Agence Nationale de la Recherche and the international exchange program CNRS-PICS France-USA. AB, YL, CB, JK, PK and LS were supported by the U.S. Department of Energy, Office of Science, Basic Energy Sciences, Materials Sciences and Engineering Division, as part of the Computational Materials Sciences Program and Center for Predictive Simulation of Functional Materials. KG and KDJ acknowledge support from the National Science Foundation under grant CHE1762337. An award of computer time was provided by the Innovative and Novel Computational Impact on Theory and Experiment (INCITE) program. All QMC results used resources of the Argonne Leadership Computing Facility, which is a DOE Office of Science User Facility supported under Contract DE-AC02-06CH11357. For the generation of the trial wavefunction, we gratefully acknowledge the computing resources provided on Bebop, a high-performance computing cluster operated by the Laboratory Computing Resource Center at Argonne National Laboratory. Sandia National Laboratories is a multi-mission laboratory managed and operated by National Technology & Engineering Solutions of Sandia, LLC,

a wholly owned subsidiary of Honeywell International Inc., for the U.S. Department of Energy National Nuclear Security Administration under contract DE-NA0003525.

REFERENCES

- ¹P. Hohenberg and W. Kohn, *Phys. Rev.* **136**, B864 (1964).
- ²W. Kohn and L. J. Sham, *Phys. Rev.* **140**, A1133 (1965).
- ³R. G. Parr and W. Yang, *Density-functional theory of atoms and molecules* (Oxford, Clarendon Press, 1989).
- ⁴L. Hedin, *Phys. Rev.* **139**, A796 (1965).
- ⁵G. Strinati, H. J. Mattausch, and W. Hanke, *Phys. Rev. Lett.* **45**, 290 (1980).
- ⁶E. E. Salpeter and H. A. Bethe, *Phys. Rev.* **84**, 1232 (1951).
- ⁷G. Strinati, *Phys. Rev. B* **29**, 5718 (1984).
- ⁸G. Strinati, *Riv. Nuovo Cimento* **11**, 1 (1988).
- ⁹R. M. Martin, *Electronic Structure: Basic Theory and Practical Methods* (Cambridge University Press, 2004).
- ¹⁰R. M. Martin, L. Reining, and D. M. Ceperley, *Interacting Electrons: Theory and Computational Approaches* (Cambridge University Press, 2016).
- ¹¹S. Di Sabatino, J. A. Berger, L. Reining, and P. Romaniello, *Phys. Rev. B* **94**, 155141 (2016).
- ¹²S. Di Sabatino, J. A. Berger, and P. Romaniello, *J. Chem. Theory Comput.* **15**, 5080 (2019).
- ¹³W. M. C. Foulkes, L. Mitas, R. J. Needs, and G. Rajagopal, *Rev. Mod. Phys.* **73**, 33 (2001).
- ¹⁴B. M. Austin, D. Y. Zubarev, and W. A. Lester, *Chem. Rev.* **112**, 263 (2012).
- ¹⁵G. H. Booth, A. J. W. Thom, and A. Alavi, *J. Chem. Phys.* **131**, 054106 (2009).
- ¹⁶G. Booth, A. Grüneis, G. Kresse, and A. Alavi, *Nature* **493**, 365 (2013).
- ¹⁷S. Zhang, J. Carlson, and J. E. Gubernatis, *Phys. Rev. B* **55**, 7464 (1997).
- ¹⁸S. Zhang and H. Krakauer, *Phys. Rev. Lett.* **90**, 136401 (2003).
- ¹⁹M. Motta, D. M. Ceperley, G. K.-L. Chan, J. A. Gomez, E. Gull, S. Guo, C. A. Jiménez-Hoyos, T. N. Lan, J. Li, F. Ma, A. J. Millis, N. V. Prokof'ev, U. Ray, G. E. Scuseria, S. Sorella, E. M. Stoudenmire, Q. Sun, I. S. Tupitsyn, S. R. White, D. Zgid, and S. Zhang (Simons Collaboration on the Many-Electron Problem), *Phys. Rev. X* **7**, 031059 (2017).
- ²⁰*Phys. Rev. X* **10**, 011041 (2020).
- ²¹W. A. Lester, L. Mitas, and B. Hammond, *Chem. Phys. Lett.* **478**, 1 (2009).

- ²²K. Nakano, C. Attaccalite, M. Barborini, L. Capriotti, M. Casula, E. Coccia, M. Dagrada, C. Genovese, Y. Luo, G. Mazzola, A. Zen, and S. Sorella, *arXiv* (2020), 2002.07401.
- ²³A. Scemama, M. Caffarel, E. Oseret, and W. Jalby, in *Lecture Notes in Computer Science* (Springer Berlin Heidelberg, 2013) pp. 118–127.
- ²⁴R. J. Needs, M. D. Towler, N. D. Drummond, P. L. Ríos, and J. R. Trail, *The Journal of Chemical Physics* **152**, 154106 (2020).
- ²⁵J. Kim, A. D. Baczewski, T. D. Beaudet, A. Benali, M. C. Bennett, M. A. Berrill, N. S. Blunt, E. J. L. Borda, M. Casula, D. M. Ceperley, S. Chiesa, B. K. Clark, R. C. Clay, K. T. Delaney, M. Dewing, K. P. Esler, H. Hao, O. Heinonen, P. R. C. Kent, J. T. Krogel, I. Kylänpää, Y. W. Li, M. G. Lopez, Y. Luo, F. D. Malone, R. M. Martin, A. Mathuriya, J. McMinis, C. A. Melton, L. Mitas, M. A. Morales, E. Neuscamman, W. D. Parker, S. D. P. Flores, N. A. Romero, B. M. Rubenstein, J. A. R. Shea, H. Shin, L. Shulenburger, A. F. Tillack, J. P. Townsend, N. M. Tubman, B. V. D. Goetz, J. E. Vincent, D. C. Yang, Y. Yang, S. Zhang, and L. Zhao, *J. Phys.: Condens. Matter* **30**, 195901 (2018).
- ²⁶P. R. C. Kent, A. Annaberdiyev, A. Benali, M. C. Bennett, E. J. L. Borda, P. Doak, H. Hao, K. D. Jordan, J. T. Krogel, I. Kylänpää, J. Lee, Y. Luo, F. D. Malone, C. A. Melton, L. Mitas, M. A. Morales, E. Neuscamman, F. A. Reboredo, B. Rubenstein, K. Saritas, S. Upadhyay, G. Wang, S. Zhang, and L. Zhao, *The Journal of Chemical Physics* **152**, 174105 (2020).
- ²⁷P. J. Reynolds, D. M. Ceperley, B. J. Alder, and W. A. Lester, *J. Chem. Phys.* **77**, 5593 (1982).
- ²⁸D. M. Ceperley, *J. Stat. Phys.* **63**, 1237 (1991).
- ²⁹A. Benali, L. Shulenburger, N. A. Romero, J. Kim, and O. A. von Lilienfeld, *J. Chem. Theory Comput.* **10**, 3417 (2014).
- ³⁰M. Dubecký, L. Mitas, and P. Jurečka, *Chemical Reviews* **116**, 5188 (2016).
- ³¹E. Giner, A. Scemama, and M. Caffarel, *Can. J. Chem.* **91**, 879 (2013).
- ³²M. A. Morales, J. McMinis, B. K. Clark, J. Kim, and G. E. Scuseria, *J. Chem. Theory Comput.* **8**, 2181 (2012).
- ³³F. R. Petruzielo, J. Toulouse, and C. J. Umrigar, *J. Chem. Phys.* **136**, 124116 (2012).
- ³⁴M. Caffarel, T. Applencourt, E. Giner, and A. Scemama, *J. Chem. Phys.* **144**, 151103 (2016).
- ³⁵A. Scemama, M. Caffarel, A. Benali, D. Jacquemin, and P.-F. Loos, *Res. Chem.* **1**, 100002 (2019).
- ³⁶A. Scemama, Y. Garniron, M. Caffarel, and P. F. Loos, *J. Chem. Theory Comput.* **14**, 1395 (2018).

- ³⁷A. Scemama, A. Benali, D. Jacquemin, M. Caffarel, and P.-F. Loos, *J. Chem. Phys.* **149**, 034108 (2018).
- ³⁸M. Caffarel, T. Applencourt, E. Giner, and A. Scemama, *ACS Symposium Series*, Vol. 1234 (American Chemical Society, 2016) Chap. 2, pp. 15–46, [arXiv:1607.06742](https://arxiv.org/abs/1607.06742).
- ³⁹A. Scemama, T. Applencourt, E. Giner, and M. Caffarel, *J. Chem. Phys.* **141**, 244110 (2014).
- ⁴⁰M. Dash, S. Moroni, A. Scemama, and C. Filippi, *J. Chem. Theory Comput.* **14**, 4176 (2018).
- ⁴¹M. Dash, J. Feldt, S. Moroni, A. Scemama, and C. Filippi, *J. Chem. Theory Comput.* **15**, 4896 (2019).
- ⁴²B. Huron, J. P. Malrieu, and P. Rancurel, *J. Chem. Phys.* **58**, 5745 (1973).
- ⁴³Y. Garniron, K. Gasperich, T. Applencourt, A. Benali, A. Ferté, J. Paquier, B. Pradines, R. Assaraf, P. Reinhardt, J. Toulouse, P. Barbaresco, N. Renon, G. David, J. P. Malrieu, M. Vénil, M. Caffarel, P. F. Loos, E. Giner, and A. Scemama, *J. Chem. Theory Comput.* **15**, 3591 (2019).
- ⁴⁴C. F. Bender and E. R. Davidson, *Phys. Rev.* **183**, 23 (1969).
- ⁴⁵J. L. Whitten and M. Hackmeyer, *The Journal of Chemical Physics* **51**, 5584 (1969), <https://doi.org/10.1063/1.1671985>.
- ⁴⁶R. J. Buenker and S. D. Peyerimhoff, *Theor. Chim. Acta* **35**, 33 (1974).
- ⁴⁷R. J. Buenker and S. D. Peyerimhoff, *Theor. Chim. Acta* **39**, 217 (1975).
- ⁴⁸R. J. Buenker, S. D. Peyerimhoff, and W. Butscher, *Mol. Phys.* **35**, 771 (1978).
- ⁴⁹S. Evangelisti, J.-P. Daudey, and J.-P. Malrieu, *Chem. Phys.* **75**, 91 (1983).
- ⁵⁰R. Cimiraglia, *The Journal of Chemical Physics* **83**, 1746 (1985), <https://doi.org/10.1063/1.449362>.
- ⁵¹R. Cimiraglia and M. Persico, *J. Comput. Chem.* **8**, 39 (1987).
- ⁵²F. Illas, J. Rubio, and J. M. Ricart, *J. Chem. Phys.* **89**, 6376 (1988).
- ⁵³A. Povill, J. Rubio, and F. Illas, *Theor. Chem. Acc.* **82**, 229 (1992).
- ⁵⁴M. L. Abrams and C. D. Sherrill, *Chem. Phys. Lett.* **412**, 121 (2005).
- ⁵⁵C. F. Bunge and R. Carbó-Dorca, *J. Chem. Phys.* **125**, 014108 (2006).
- ⁵⁶L. Bytautas and K. Ruedenberg, *Chem. Phys.* **356**, 64 (2009).
- ⁵⁷M. Caffarel, E. Giner, A. Scemama, and A. Ramírez-Solís, *J. Chem. Theory Comput.* **10**, 5286 (2014).
- ⁵⁸E. Giner, A. Scemama, and M. Caffarel, *J. Chem. Phys.* **142**, 044115 (2015).
- ⁵⁹Y. Garniron, A. Scemama, P.-F. Loos, and M. Caffarel, *J. Chem. Phys.* **147**, 034101 (2017).

- ⁶⁰A. A. Holmes, N. M. Tubman, and C. J. Umrigar, *Journal of Chemical Theory and Computation* **12**, 3674 (2016), pMID: 27428771, <http://dx.doi.org/10.1021/acs.jctc.6b00407>.
- ⁶¹S. Sharma, A. A. Holmes, G. Jeanmairet, A. Alavi, and C. J. Umrigar, *J. Chem. Theory Comput.* **13**, 1595 (2017).
- ⁶²A. A. Holmes, C. J. Umrigar, and S. Sharma, *J. Chem. Phys.* **147**, 164111 (2017).
- ⁶³A. D. Chien, A. A. Holmes, M. Otten, C. J. Umrigar, S. Sharma, and P. M. Zimmerman, *J. Phys. Chem. A* **122**, 2714 (2018).
- ⁶⁴P.-F. Loos, A. Scemama, A. Blondel, Y. Garniron, M. Caffarel, and D. Jacquemin, *J. Chem. Theory Comput.* **14**, 4360 (2018).
- ⁶⁵Y. Garniron, A. Scemama, E. Giner, M. Caffarel, and P. F. Loos, *J. Chem. Phys.* **149**, 064103 (2018).
- ⁶⁶F. A. Evangelista, *J. Chem. Phys.* **140**, 124114 (2014).
- ⁶⁷J. B. Schriber and F. A. Evangelista, *J. Chem. Phys.* **144**, 161106 (2016).
- ⁶⁸J. B. Schriber and F. A. Evangelista, *J. Chem. Theory Comput.* **13**, 5354 (2017).
- ⁶⁹W. Liu and M. R. Hoffmann, *J. Chem. Theory Comput.* **12**, 1169 (2016).
- ⁷⁰M. C. Per and D. M. Cleland, *J. Chem. Phys.* **146**, 164101 (2017).
- ⁷¹Y. Ohtsuka and J. ya Hasegawa, *J. Chem. Phys.* **147**, 034102 (2017).
- ⁷²P. M. Zimmerman, *J. Chem. Phys.* **146**, 104102 (2017).
- ⁷³J. Li, M. Otten, A. A. Holmes, S. Sharma, and C. J. Umrigar, *J. Chem. Phys.* **149**, 214110 (2018).
- ⁷⁴J. P. Coe, *J. Chem. Theory Comput.* **14**, 5739 (2018).
- ⁷⁵P. F. Loos, M. Boggio-Pasqua, A. Scemama, M. Caffarel, and D. Jacquemin, *J. Chem. Theory Comput.* **15**, in press (2019).
- ⁷⁶P. F. Loos, A. Scemama, and D. Jacquemin, *J. Phys. Chem. Lett.* , 2374 (2020).
- ⁷⁷P. F. Loos, F. Lipparini, M. Boggio-Pasqua, A. Scemama, and D. Jacquemin, *J. Chem. Theory Comput.* **16**, 1711 (2020).
- ⁷⁸J. S. Anderson, F. Heidar-Zadeh, and P. W. Ayers, *Comput. Theor. Chem.* **1142**, 66 (2018).
- ⁷⁹J. Kolorenč and L. Mitás, *Reports on Progress in Physics* **74**, 026502 (2011).
- ⁸⁰S. W. de Leeuw, J. W. Perram, and E. R. Smith, *Proc. R. Soc. Lond. Ser. A* **373**, 27 (1980).
- ⁸¹M. P. Allen and D. J. Tildesley, *Computer Simulation of Liquids* (Oxford: Oxford University Press, 1989).
- ⁸²H. J. Monkhorst and J. D. Pack, *Phys. Rev. B* **13**, 5188 (1976).

- ⁸³P. M. W. Gill, M. Head-Gordon, and J. A. Pople, *Int. J. Quantum Chem.* **36**, 269 (1989).
- ⁸⁴P. M. W. Gill and J. A. Pople, *Int. J. Quantum Chem.* **40**, 753 (1991).
- ⁸⁵J. McClain, Q. Sun, G. K.-L. Chan, and T. C. Berkelbach, *J. Chem. Theory Comput.* **13**, 1209 (2017).
- ⁸⁶A. Szabo and N. S. Ostlund, *Modern quantum chemistry* (McGraw-Hill, New York, 1989).
- ⁸⁷A. Scemama and E. Giner, *arXiv [physics.comp-ph]*, 1311.6244 (2013).
- ⁸⁸Q. Sun, T. C. Berkelbach, N. S. Blunt, G. H. Booth, S. Guo, Z. Li, J. Liu, J. D. McClain, E. R. Sayfutyarova, S. Sharma, S. Wouters, and G. K. Chan, *WIREs Comput. Mol. Sci.* **8**, e1340 (2017).
- ⁸⁹C. Lin, F. H. Zong, and D. M. Ceperley, *Phys. Rev. E* **64**, 016702 (2001).
- ⁹⁰M. Burkatzki, C. Filippi, and M. Dolg, *J. Chem. Phys.* **126**, 234105 (2007).
- ⁹¹M. Burkatzki, C. Filippi, and M. Dolg, *J. Chem. Phys.* **129**, 164115 (2008).
- ⁹²M. Casula, *Phys. Rev. B* **74**, 161102 (2006).
- ⁹³C. J. Umrigar, J. Toulouse, C. Filippi, S. Sorella, and R. G. Hennig, *Phys. Rev. Lett.* **98**, 110201 (2007).
- ⁹⁴J. P. Perdew and A. Zunger, *Physical Review B* **23**, 5048 (1981).
- ⁹⁵J. P. Perdew, K. Burke, and M. Ernzerhof, *Phys. Rev. Lett.* **77**, 3865 (1996).
- ⁹⁶A. D. Becke, *The Journal of Chemical Physics* **98**, 5648 (1993), <https://doi.org/10.1063/1.464913>.
- ⁹⁷C. Lee, W. Yang, and R. G. Parr, *Phys. Rev. B* **37**, 785 (1988).
- ⁹⁸S. H. Vosko, L. Wilk, and M. Nusair, *Canadian Journal of Physics* **58**, 1200 (1980), <https://doi.org/10.1139/p80-159>.
- ⁹⁹P. J. Stephens, F. J. Devlin, C. F. Chabalowski, and M. J. Frisch, *The Journal of Physical Chemistry* **98**, 11623 (1994), <https://doi.org/10.1021/j100096a001>.
- ¹⁰⁰H. Shin, S. Kang, J. Koo, H. Lee, J. Kim, and Y. Kwon, *J. Chem. Phys.* **140**, 114702 (2014).
- ¹⁰¹Data of Ref. 100 kindly provided by the authors.
- ¹⁰²L. Schimka, J. Harl, and G. Kresse, *The Journal of Chemical Physics* **134**, 024116 (2011).
- ¹⁰³M. W. Chase and NIST, *JANAF Thermodynamic Tables*, Vol. 14 (American Chemical Society, [Washington, D.C.], 1985) pp. 61–65.
- ¹⁰⁴A. Scemama, T. Applencourt, E. Giner, and M. Caffarel, *J. Comput. Chem.* **37**, 1866 (2016).
- ¹⁰⁵R. Q. Hood, P. R. C. Kent, R. J. Needs, and P. R. Briddon, *Physical Review Letters* **91** (2003), [10.1103/physrevlett.91.076403](https://doi.org/10.1103/physrevlett.91.076403).

- ¹⁰⁶P. L. Ríos, A. Ma, N. D. Drummond, M. D. Towler, and R. J. Needs, *Physical Review E* **74** (2006), [10.1103/physreve.74.066701](https://doi.org/10.1103/physreve.74.066701).
- ¹⁰⁷T. J. and U. C. J., *The Journal of Chemical Physics* **128**, 174101 (2008), <https://doi.org/10.1063/1.2908237>.
- ¹⁰⁸E. Giner, R. Assaraf, and J. Toulouse, *Molecular Physics* **114**, 910 (2016), <https://doi.org/10.1080/00268976.2016.1149630>.
- ¹⁰⁹C. Genovese, T. Shirakawa, K. Nakano, and S. Sorella, *arXiv* (2020), [2002.03347](https://arxiv.org/abs/2002.03347).

Supplementary Material for “Towards a Systematic Improvement of the Fixed-Node Approximation in Diffusion Monte Carlo for Solids”

Anouar Benali,^{1, a)} Kevin Gasperich,² Thomas Applencourt,³ Ye Luo,¹ M. Chandler Bennett,⁴ Luke Shulenburger,⁵ Paul R. C. Kent,^{6,7} Jaron T. Krogel,⁴ Kenneth D. Jordan,² Pierre-François Loos,⁸ Anthony Scemama,⁸ and Michel Caffarel^{8, b)}

¹⁾Computational Sciences Division, Argonne National Laboratory, Argonne, IL 60439, United States

²⁾Department of Chemistry, University of Pittsburgh, Pittsburgh, Pennsylvania 15260, United States

³⁾Argonne Leadership Computing Facility, Argonne National Laboratory, Argonne, IL 60439, United States

⁴⁾Materials Science and Technology Division, Oak Ridge National Laboratory, Oak Ridge, TN 37831, United States

⁵⁾HEDP Theory Department, Sandia National Laboratories, Albuquerque, New Mexico 87185, USA

⁶⁾Center for Nanophase Materials Sciences, Oak Ridge National Laboratory, Oak Ridge, TN 37831, United States

⁷⁾Computational Sciences and Engineering Division, Oak Ridge National Laboratory, Oak Ridge, TN 37831, United States

⁸⁾Laboratoire de Chimie et Physique Quantiques, Université de Toulouse, CNRS, UPS, France

TABLE I. Raw data associated with Fig. 1 of the main text. SD-DMC energy of the $1 \times 1 \times 1$ diamond cell in hartree computed at the Γ point using SD trial wave functions built with various orbitals (LDA, PBE, B3LYP, and HF) and the BFD-vDZ or BFD-vTZ basis sets. The SD-DMC energy obtained using a large plane wave basis set and LDA orbitals is also reported.

DMC nodal surface	BFD-vDZ	BFD-vTZ	Plane wave
LDA	-10.524 4(6)	-10.531 2(6)	-10.531 6(2)
PBE	-10.525 0(7)	-10.530 0(6)	
B3LYP	-10.525 1(3)	-10.530 3(6)	
HF	-10.523 0(4)	-10.530 0(6)	

^{a)}Electronic mail: benali@anl.gov

^{b)}Electronic mail: caffarel@irsamc.ups-tlse.fr

TABLE II. Raw data associated with Fig. 2 of the main text. CIPSI calculations for the $1 \times 1 \times 1$ diamond cell computed at the Γ point. Zeroth-order energy E_{var} and its second-order corrected value $E_{\text{var}} + E_{\text{PT2}}$ computed with the BFD-vTZ basis set using HF orbitals (black) and B3LYP orbitals as a function of the number of determinants in the reference space N_{det} .

Trial wave function built with B3LYP orbitals			Trial wave function built with HF orbitals		
N_{det}	E_{var}	$E_{\text{var}} + E_{\text{PT2}}$	N_{det}	E_{var}	$E_{\text{var}} + E_{\text{PT2}}$
1	-10.256 500	-10.715 659(0)	1	-10.264 922	-10.665 580(0)
2	-10.270 720	-10.680 510(0)	2	-10.286 108	-10.635 618(0)
4	-10.287 604	-10.646 809(0)	4	-10.317 600	-10.603 077(0)
12	-10.302 464	-10.624 797(0)	16	-10.330 562	-10.597 064(40)
26	-10.320 253	-10.610 121(68)	33	-10.348 435	-10.589 059(35)
44	-10.342 205	-10.596 419(44)	63	-10.372 320	-10.579 472(21)
89	-10.370 832	-10.585 930(41)	123	-10.396 530	-10.571 746(25)
186	-10.399 763	-10.574 829(28)	260	-10.421 103	-10.566 893(41)
354	-10.428 321	-10.569 508(30)	527	-10.448 298	-10.563 121(29)
649	-10.455 603	-10.565 942(33)	977	-10.474 204	-10.561 915(2)
1 328	-10.480 127	-10.564 005(9)	1 922	-10.496 143	-10.560 772(7)
2 564	-10.501 270	-10.562 202(5)	3 786	-10.513 817	-10.560 327(7)
5 270	-10.518 185	-10.561 202(4)	7 799	-10.527 755	-10.560 453(3)
11 380	-10.531 109	-10.560 784(2)	16 858	-10.538 165	-10.560 518(3)
24 157	-10.540 197	-10.560 795(5)	36 731	-10.545 337	-10.560 666(1)
58 210	-10.546 579	-10.560 853(10)	93 865	-10.550 501	-10.560 721(1)
153 319	-10.551 656	-10.560 836(8)	251 136	-10.554 414	-10.560 740(4)
409 317	-10.555 405	-10.560 813(8)	699 998	-10.557 172	-10.560 746(7)
1 120 101	-10.557 898	-10.560 786(9)	1 831 452	-10.558 815	-10.560 770(9)
3 000 000	-10.559 339	-10.560 769(6)	2 684 325	-10.559 261	-10.560 757(10)

TABLE III. Raw data associated with Fig. 3 of the main text. Error in DMC energy (in hartree/atom) as a function of the number of orbitals kept in the restricted active space (RAS) for trial wave functions built with HF orbitals ($1 \times 1 \times 1$ cell) or B3LYP orbitals ($1 \times 1 \times 1$ and $2 \times 1 \times 1$ cells). All these calculations are performed with the BFD-vTZ basis set.

Size of RAS	$1 \times 1 \times 1$ (HF orb.)		$1 \times 1 \times 1$ (B3LYP orb.)		$2 \times 1 \times 1$ (B3LYP orb.)	
	N_{det}	DMC energy	N_{det}	DMC energy	N_{det}	DMC energy
10	5 319	-10.560 0(4)	9 296	-10.562 8(4)	1 168 596	-21.866 8(15)
16	188 120	-10.564 9(5)	165 343	-10.565 6(4)		
20	702 164	-10.573 0(4)	538 259	-10.572 9(6)	1 996 113	-21.887 1(9)
30	1 020 290	-10.574 6(6)	1 510 556	-10.579 6(9)	1 072 503	-21.891 7(10)
40	1 000 000	-10.578 4(4)	1 332 184	-10.580 8(12)	2 355 783	-21.896 5(14)
50	1 666 328	-10.580 0(10)	1 211 711	-10.580 4(11)	2 000 000	-21.897 9(7)
58	1 831 452	-10.581 7(5)	1 137 782	-10.580 6(4)	1 827 608	-21.897 4(10)

TABLE IV. Raw data associated with Fig. 5 of the main text. SD- and MD-DMC total energies (in hartree/cell) as a function of the system size N . Energies calculated at the Γ point or by twist-averaging. Each set of energies (SD or MD) are fitted simultaneously (see main text for more details).

Cell ($n \times n \times n$)	System size ($N = n^3$)	SD-DMC energies		MD-DMC energies	
		Γ point	Twist-averaged	Γ point	Twist-averaged
$2 \times 2 \times 2$	8	-11.291 5(2)	-11.421 73(8)	-11.316 8(4)	-11.441 11(8)
$3 \times 3 \times 2$	18			-11.388 6(2)	
$3 \times 3 \times 3$	27	-11.386 4(2)	-11.407 8(7)	-11.403 4(3)	-11.426 4(4)
$4 \times 4 \times 4$	64	-11.397 2(1)	-11.402 0(5)	-11.418 4(4)	-11.419 9(4)
Extrapolated	∞	-11.398 6(2)	-11.398 6(2)	-11.424 6(4)	-11.424 6(4)

TABLE V. Raw data associated with Fig. 6 of the main text. Twist-averaged SD-DMC and MD-DMC energies (in hartree/cell) for the $2 \times 2 \times 2$ supercell as a function of the twist index (16 independent twists out of the 216 k -point grid). The exact and approximate calculations computed are reported (see main text).

Twist index	SD-DMC energy		MD-DMC energy	
	Exact	Approx.	Exact	Approx.
0	-11.291 5(2)	-11.291 5(2)	-11.316 7(4)	-11.316 8(4)
1	-11.328 8(3)	-11.327 2(3)	-11.336 3(2)	-11.352 4(2)
2	-11.392 1(5)	-11.391 7(5)	-11.404 3(4)	-11.416 9(4)
3	-11.418 8(3)	-11.418 8(3)	-11.425 5(2)	-11.444 0(2)
4	-11.340 0(2)	-11.340 0(2)	-11.357 8(1)	-11.365 2(1)
5	-11.393 9(3)	-11.394 8(3)	-11.417 3(3)	-11.420 0(3)
6	-11.430 5(2)	-11.433 1(2)	-11.445 4(3)	-11.458 3(3)
7	-11.422 6(3)	-11.424 3(3)	-11.447 6(3)	-11.449 5(3)
8	-11.374 1(2)	-11.374 1(2)	-11.393 6(5)	-11.399 3(5)
9	-11.421 0(4)	-11.423 0(4)	-11.436 2(3)	-11.448 2(3)
10	-11.450 0(3)	-11.452 1(3)	-11.469 2(2)	-11.477 4(2)
11	-11.451 6(4)	-11.454 9(4)	-11.478 8(4)	-11.480 1(4)
12	-11.433 4(3)	-11.435 6(3)	-11.444 9(3)	-11.460 8(3)
13	-11.453 1(1)	-11.455 3(1)	-11.482 2(2)	-11.480 5(2)
14	-11.455 4(2)	-11.457 6(2)	-11.472 6(2)	-11.482 8(2)
15	-11.459 7(3)	-11.463 6(3)	-11.477 2(4)	-11.488 8(4)

TABLE VI. DMC total energies (in hartree/cell) computed at the Γ point for the $1 \times 1 \times 1$ diamond primitive cell as a function of the truncation threshold ϵ on the coefficients of the full CIPSI wave function ($\epsilon = 0$) computed within the FCI space with the BFD-vTZ basis set. The full CIPSI wave function is obtained by stopping the selection process when the number of determinants exceeds about 1 million. The number of determinants in the trial wave function, the intrinsic variance the number of blocks to reach DMC convergence the efficiency of the run and the total run time are also reported for each value of ϵ . we define the efficiency as $\frac{1}{\sigma^2 t}$, where σ is the error bar and t is the total time (number of walkers \times wall time).

Truncation threshold ϵ	FCI space					
	# determinants	DMC energy	Intrinsic variance	# blocks	Efficiency	KNL core-hours
10^{-2}	178	-10.5638(3)	0.2428(4)	949	268.89	2457
10^{-3}	4124	-10.5707(3)	0.2010(1)	949	183.29	3550
10^{-4}	80864	-10.5791(4)	0.1730(2)	646	31.81	11741
10^{-5}	738998	-10.5812(3)	0.1382(7)	335	8.80	32768
$\epsilon = 0$	1043197	-10.5817(4)	0.1372(8)	194	9.00	32768

TABLE VII. DMC total energies (in hartree/cell) computed at the Γ point for the $1 \times 1 \times 1$ diamond primitive cell as a function of the truncation threshold ϵ on the coefficients of the full CIPSI wave function ($\epsilon = 0$) computed within the restricted CAS-CI space with the BFD-vTZ basis set. The full CIPSI wave function is obtained by stopping the selection process when the number of determinants exceeds about 1 million. The number of determinants in the trial wave function, the intrinsic variance the number of blocks to reach DMC convergence, the efficiency of the run and the total run time are also reported for each value of ϵ . we define the efficiency as $\frac{1}{\sigma^2 t}$, where σ is the error bar and t is the total time (number of walkers \times wall time).

Truncation threshold ϵ	CAS-CI space					
	# determinants	DMC energy	Intrinsic variance	# blocks	Efficiency	KNL core-hours
10^{-2}	200	-10.5633(2)	0.2399(5)	949	553.30	2457
10^{-3}	3204	-10.5694(3)	0.1950(2)	949	535.32	3003
10^{-4}	57990	-10.5754(7)	0.1720(2)	195	518.59	17476
10^{-5}	578025	-10.5776(4)	0.16384(5)	600	7.49	32768
$\epsilon = 0$	1282995	-10.5788(8)	0.16338(9)	206	2.17	32768